Rapid sediment deposition and fine-scale strata formation in the Hudson estuary

Peter Traykovski and Rocky Geyer

Applied Ocean Physics and Engineering Department, Woods Hole Oceanographic Institution, Woods Hole, Massachusetts, USA

Chris Sommerfield

College of Marine Studies, University of Delaware, Lewes, Delaware, USA

Received 17 September 2003; revised 18 February 2004; accepted 25 February 2004; published 21 April 2004.

[1] A 9 month time series of tripod-mounted optical and acoustic measurements of sediment concentration and bed elevation was used to examine depositional processes in relationship to hydrodynamic variables in the Hudson River estuary. A series of cores was also taken directly under and adjacent to the acoustic measurements to examine the relation between the depositional processes and the resulting fine-scale stratigraphy. The measurements reveal that deposition occurs as a result of sediment flux convergence behind a salinity front and that the accumulation rates are sufficient to deposit up to 25 cm of new high-porosity sediment in a single ebb-tidal phase. Subsequent dewatering and erosion reduces the thickness of the initial deposit to several centimeters. These depositional events were only observed on spring tides. Ten depositional events during two spring tidal cycles produced a seasonal deposit of 18 cm, consistent with estimates of seasonal deposition from cores. A proxy for near-bed suspended grain size variations was estimated from the combined acoustic and optical measurements, implying that the erosional processes resuspend only the finer-grained sediments, thus leaving behind silt and very fine grained sand beds. The thickness of the deposited homogenous clayey silt beds, and the vertical separation between beds interlaminated with silt and very fine sand, are roughly consistent with the acoustic measurements of changes in bed elevations during deposition and erosion. The variability in individual bed thickness is the result of variations of processes over an individual tidal cycle and is not a product of variations over the spring neap fortnightly timescale. *INDEX TERMS:* 3022 Marine Geology and Geophysics: Marine sediments—processes and transport; 4235 Oceanography: General: Estuarine processes; 4558 Oceanography: Physical: Sediment transport; *KEYWORDS:* sediment transport, estuarine processes, fluid mud

Citation: Traykovski, P., R. Geyer, and C. Sommerfield (2004), Rapid sediment deposition and fine-scale strata formation in the Hudson estuary, *J. Geophys. Res.*, *109*, F02004, doi:10.1029/2003JF000096.

1. Introduction

[2] Understanding of the relationships between sediment resuspension, transport and deposition processes, short-timescale stratigraphy, and the spatial distribution of the stratigraphy produced by these processes has been one of the often elusive goals of modern sediment transport studies [e.g., *Nittrouer*, 1999]. An understanding of these relationships allows one to better interpret the longer-timescale geological record and places the modern dynamic process in context of the longer-timescale evolution of the system in question. For instance, *Geyer et al.* [2000], *Traykovski et al.* [2000], and *Wheatcroft and Borgeld* [2000] were able to relate the deposition pattern of riverine sediment on the continental shelf off the Eel River to shelf sediment transport processes involving surface gravity waves. In this study we will use a similar approach to examine the processes leading to formation of small-scale stratigraphy in the estuarine turbidity maximum (ETM) of the Hudson River estuary.

[3] Trapping of suspended sediment at an ETM is a well-known phenomenon [*Glangeaud*, 1938; *Meade*, 1969]. In general, it results from a combination of a residual hydrodynamic convergence and adequate sediment supply into this convergence. The convergence is a result of landward flowing, dense, salty water near the bottom, with seaward flowing fresh water above it [*Postma*, 1967]. Enhanced settling of particles due to flocculation [*Postma*, 1967; *Gibbs et al.*, 1989; *Lick and Huang*, 1993] and reduction of turbulence due to stratification [*Geyer*, 1993] tends to keep the particles near the bed where the convergence is strongest. If the supply of sediment to this trapping region is greater than the amount that can be resuspended, deposits

0148-0227/04/2003JF000096$09.00

will form under the ETM [*Wellershaus*, 1981]. These deposits often take the form of patches of fluid mud, which can be either mobile or stationary [*Ross and Mehta*, 1989] and which can consolidate into bed material.

[4] In tidal environments, these deposits reflect the variations in tidal energy through sedimentary structures known as tidal rythmites or tidalites, which are alternating beds of fine sand, silt, and mud that may be homogeneous or internally laminated. While the presence of these rythmites has been observed in many locations and they have been shown to be related to tidal processes, the exact pattern of deposition and erosion over the tidal timescale that creates these structures has not been well documented. One of the best examples of relating fine-scale stratigraphy to dynamic processes is the study by *Jaeger and Nittrouer* [1995] on the Amazon River shelf. Although this is not precisely an estuary, the high freshwater discharge of the Amazon River results in an estuarine-like circulation on the inner shelf. *Jaeger and Nittrouer* [1995] found that thick mud beds are deposited during neap tides and thinner mud beds or sand-mud laminated beds are formed during spring tides.

[5] *Woodruff et al.* [2001] observed thick (>20 cm) deposits in the Hudson River ETM that occurred on timescales of weeks to months, based on the presence of the radionuclide Be-7 in the sediment (half-life 53 days). They hypothesize that the mud deposits were spatially localized (with scales of several hundred meters), occurring as a result of intense frontal trapping. They further suggest that the alternation of silty and muddy layers may reflect flood versus ebb deposition, with homogeneous layers as thick as 1–4 cm representing individual episodes of settling. However, the actual process of convergence and deposition was not observed in that study. *Hori et al.* [2001] observed sand-mud couplet laminations in the Changjiang estuary. They related the variation in thickness of the couplets to spring neap tidal amplitude variations, with spring tides producing thicker couplets. Again, the correlation of bedding to the actual hydrodynamic process was inferred and not directly observed.

[6] This paper presents direct observations of erosion and deposition processes in the Hudson River estuary using tripod-mounted acoustic instruments that measure changes in bottom elevation as well as near-bed suspended sediment concentrations. Sediment cores obtained in conjunction with the tripod measurements provide a comparison of the observed sedimentary structure with the time course of sediment deposition and erosion.

2. Site Description and Background

[7] The Hudson River estuary is a long, relatively straight and narrow incised river valley. Tidal conditions extend 250 km from the entrance at New York Harbor to the confluence of the Mohawk and Upper Hudson Rivers near Troy, New York; however, the extent of salt water is restricted to the first 100 km of the tidal river during low flow and less than 30 km during freshet conditions. The channel of the lower estuary is straight, although the bathymetry is laterally asymmetric (Figure 1). The west side of the lower estuary is shallow, ~8–12 m deep, while the channel on the east side of the estuary has depths

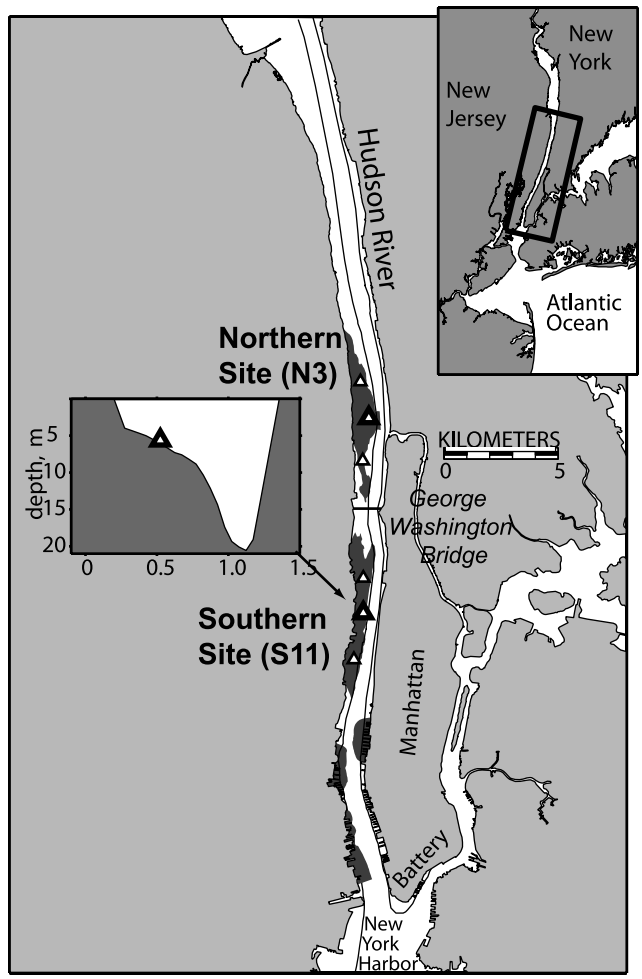

Figure 1. Site map and bathymetry and depositional (dark fill) sites from *Woodruff et al.* [2001]. Mooring and tripod locations are shown as triangles.

ranging from 15 to 20 m. The bathymetry also has moderate along-channel variability, with multiple sills and depressions of several meters amplitude.

[8] The Hudson estuary is "partially mixed," with vertical salinity differences ranging from 2 to 15 practical salinity units (psu) [*Geyer et al.*, 2001]. Weak stratification occurs during spring tides, and strong stratification occurs during neaps and high river flow conditions. Maximum surface tidal velocities in the lower estuary are 100–150 cm s^{-1} during spring tides and are reduced to 60–80 cm s^{-1} during neap tides. Near-bed velocities are 110–130 cm s^{-1} during spring tides and 60–80 cm s^{-1} during neap tides. River discharge ranges from 100 m^3 s^{-1} during low-flow conditions to 2000 m^3 s^{-1} during typical spring freshet conditions. The river flow and estuarine circulation produce tidally averaged surface velocities in the lower estuary of ~10 cm s^{-1} in the seaward direction during low flow conditions and over 100 cm s^{-1} during freshets. Near-bottom tidally averaged currents are landward at 5–10 cm s^{-1} in the eastern channel. Near-bottom tidally averaged currents on the western shoals are seaward at 5–10 cm s^{-1} during low flow and are seaward at 30–50 cm s^{-1} during freshets.

[9] The flow and stratification conditions in the Hudson estuary result in the trapping of sediment at an ETM in the lower estuary [*Woodruff et al.*, 2001; *Geyer et al.*, 2001]. Modeling studies by *Geyer et al.* [1998] suggest that the trapping process is influenced by frontal convergence as well as by lateral circulation processes, producing a pattern of sediment trapping that is intensified on the west side of the estuary. Coring studies by *Woodruff et al.* [2001] indicate rapid sediment accumulation in the ETM following the spring freshet, with seasonal accumulations of 20 cm or more in localized areas. These deposits form on the shallow western side of the estuary, both south and north of the George Washington Bridge. These sites, referred to as S-11 and N-3 in *Woodruff et al.* [2001], will henceforth be referred to as the southern and northern depositional sites in this paper. The coring observations of *Woodruff et al.* [2001] as well as time series measurements by *Geyer et al.* [2001] indicate that the sediment accumulation in the ETM is associated with northward transport following the spring freshet and that there actually may be sediment erosion in the ETM zone during the freshet. The pattern of sediment flux suggested by these observations as well as from radionuclide studies by *Feng et al.* [1999] is a southward flux into the lower estuary and New York Harbor during freshet conditions, followed by remobilization, northward transport, and trapping in the ETM during the months following the freshet. The time series observations of *Geyer et al.* [2001] indicate that this northward transport occurs almost exclusively during spring tide conditions, when sediment resuspension is maximal. These observations did not yield any information about the actual timing or mechanisms of sediment trapping within the ETM zone.

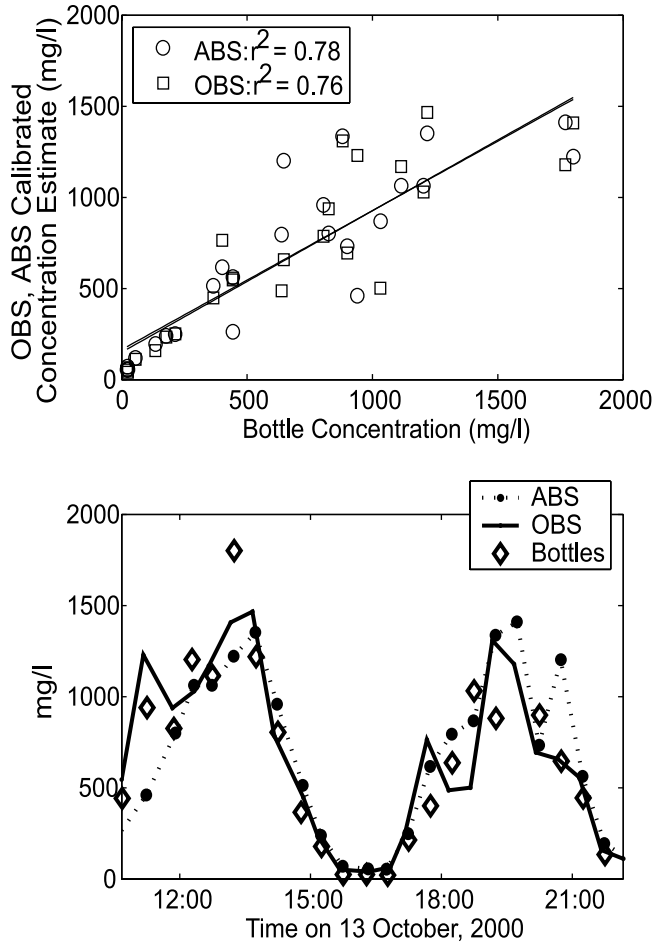

Figure 2. (top) Calibrated optical backscattering sensor (OBS) and acoustic backscattering sensor (ABS) concentration estimates from the southern depositional site tripod versus bottle samples taken near the tripod at 0.5 meters above bottom (mab). (bottom) ABS and OBS concentration estimates and bottle concentration time series.

3. Observation Program

[10] An observation program was conducted between the fall of 2000 and the summer of 2001 to document the erosion and deposition processes in the Hudson ETM over a seasonal cycle. Two tripods, each with surface moorings, were deployed from 5 October 2000 to 26 June 2001, with a turnaround for cleaning and data recovery on 14 March 2001. The tripods were deployed north and south of the George Washington Bridge (at depths of 6 and 9 m, respectively) in the center of depositional areas identified by *Woodruff et al.* [2001]. Each tripod included an acoustic backscattering sensor (ABS), which measured changes in bed elevation under the tripod to infer deposition and erosion. In order to ensure that the tripods provided a fixed reference frame for measuring erosion and deposition, poles were driven 4–5 m into the sediment at each tripod leg. The tripods also included Nortek acoustic Doppler velocimeters (ADVs) for high-resolution current and turbulence measurements near the bed (1.2 m above bed), Laser In-Situ Scattering and Transmissometry (LISST) sensors located 1.0 m above the bed to estimate suspended particle size, upward looking acoustic Doppler current profilers (ADCPs), salinity, temperature, and pressure sensors, and vertical arrays of two to three optical backscattering sensors (OBS). During the turnaround, smaller tripods were deployed north and south of the central tripod at both sites. These smaller tripods, which included current meters, salinity, temperature, and OBS sensors, were deployed to estimate convergence of suspended sediment flux and to identify the salinity front associated with the estuarine turbidity maximum. The surface moorings located near each central tripod contained OBS sensors and salinity and temperature sensors.

3.1. Acoustic Backscattering Sediment Measurements

[11] The ABS system measures vertical profiles of acoustic backscattered intensity with three frequencies (1, 2.5, and 5 MHz) in 1 cm range bins over a total range of 128 cm. A burst sampling mode was used with 600 s bursts every half hour to resolve tidal and turbulence timescales. Individual profiles, sampled at rate of 64 Hz, were averaged and saved at 1 Hz. The range dependence due to spherical spreading and near-field effects was corrected for as described by *Thorne et al.* [1993]. The backscattered intensity was calibrated against sediment concentration from in situ bottle samples using a linear regression as shown in Figure 2. Acoustic scattering from sediment is linearly related to backscattered intensity for a constant grain size distribution; however, it is known to be sensitive to grain

size variations. Sediment grain sizes found in suspension at the Hudson ETM are typically smaller than fine sand (125 mm). Mean, disaggregated grain size for bottom samples at the southern site range from 5 to 20 μm (i.e., clayey silt). These grain sizes are much smaller than the inverse acoustic wave number ($a \ll 1/k$, where a is grain radius) for all three frequencies; thus the backscattered intensity dependence on grain size is in the Raleigh regime and is proportional to a^3 for single grains [*Lynch et al.*, 1994]. This implies that the acoustic scattering is most sensitive to the larger grain sizes in suspension. Most of the particles found in suspension at the Hudson ETM are not single grains but are flocculates of many smaller particles [*Gibbs et al.*, 1994].

[12] The dependence of scattered energy on floc size has not been examined in detail; however, acoustics should respond most strongly to large, dense particles or aggregates containing large, dense particles. *Fugate and Friedrichs* [2002] showed that the relation between acoustic backscattered intensity and mass concentration from a Sontek ADV was relatively insensitive to floc size, and thus there was a linear relation between mass concentration and acoustic backscatter for flocs. The linear calibration shown in Figure 2 effectively averages over variability due to particle size. Estimates of concentration in individual profiles potentially have error on the order of the error in the calibration (±25%) due to particle size variability. This assumes that particle size distribution variability in subsequent tidal cycles is similar to that in the calibration tidal cycle. Because all three acoustic frequencies have the same dependence on grain size, only the 1.0 MHz channel is used to estimate concentration because it has the lowest attenuation due to sediment. During periods of high sediment concentration a recursive algorithm is used to account for attenuation of the acoustic signal due to sediment [*Thorne et al.*, 1993]. Using data from a tank settling experiment, it was found that this algorithm failed to converge at concentrations over 30 g L^{-1} with the 1.0 MHz sensor and thus was only used when concentrations were estimated to be between 1 and 30 g L^{-1}. At lower concentrations, for the 1 MHz transducer, the attenuation correction was very small and thus was not used.

3.2. Settling Tank Experiments

[13] A set of tank experiments was conducted to determine the response of the 1 MHz sensor to high concentrations of sediment. An 80 cm deep, 400 L volume tank was filled with water and 12 kg of sediment from the southern depositional site. The tank was stirred to resuspend the sediment to a uniform concentration (C) of ~30 g L^{-1} and then was allowed to settle for 3 hours while acoustic backscatter profiles were taken (Figure 3). Water and sediment samples were also taken at four depths (9, 19, 29, and 39 cm, then 3, 9, 19, and 29 cm for the last three profiles) to measure sediment mass concentration. After 3hours in this experiment a 15-cm-thick mud layer with concentration of 250 g L^{-1} at the bottom and 150 g L^{-1} at the top was present at the bottom of the tank. The experiment was repeated with several different initial mass concentrations to create layers of varying thickness. These tank experiments helped us understand the rate of attenuation of 1.0 MHz acoustic energy in recently deposited mud. It was found that 1.0 Mhz acoustic energy could penetrate, scatter off an interface at the bottom of the tank, and then return through thin (5–10 cm) layers of recently deposited mud (150–250 g L^{-1}), but if the layers were thicker (20–30 cm), the amount of acoustic energy that was returned from the bottom of the tank was not detectable by this system.

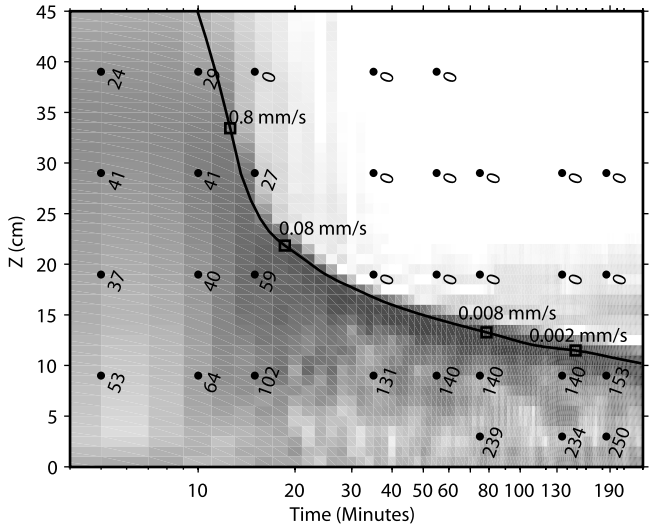

Figure 3. Time series of backscatter from a settling tank experiment. The gray shading represents an uncalibrated log of acoustic intensity. The line indicates the approximate location of the lutocline and was used to estimate the lutocline settling rate. The dots and numbers represent mass concentrations from suction samples. Rates of lutocline settling estimated by the derivative of the lutocline curve are shown at the locations indicated by squares and range from 0.8 to 0.002 mm s^{-1}. The scattering above the lutocline (12–22 cm) after the beginning of the record is from sidelobe interactions with the side of the tank. Weak scattering from the accumulated mud at the bottom of the tank at 2–3 cm is visible toward the end of the record.

[14] Since the lutocline (mud water interface) is visible in the acoustic record, the lutocline curve can be used to estimate hindered settling rates (w_{sh}) for various concentrations, as shown in Figure 3. On the basis of these data, parameters can be found for a hindered settling relation of the form suggested by *Richardson and Zaki* [1954]:

$$w_{sh} = w_{s0}(1 - k_2 C)^m. \quad (1)$$

Here the fall velocity of the large flocs without hindered settling effects (w_{s0}) is estimated as 1.6 mm s^{-1}, and $k_2 = 1/C_{gel}$ [*Ross and Mehta*, 1989] is estimated as 1/160 (g L^{-1})$^{-1}$. C_{gel} is the concentration where the interparticle forces result in a nearly immobile bed. Other formulations exist for the hindered settling velocity that are more closely related to the physics of the process [*Winterwerp*, 2002], but this one provided the best empirical fit to the data with only two fitting parameters (k_2 and w_{s0}). The exponent m has a theoretical value of 5 and thus is not a fitting parameter [*Ross and Mehta*, 1989]. Generally, all the formulations

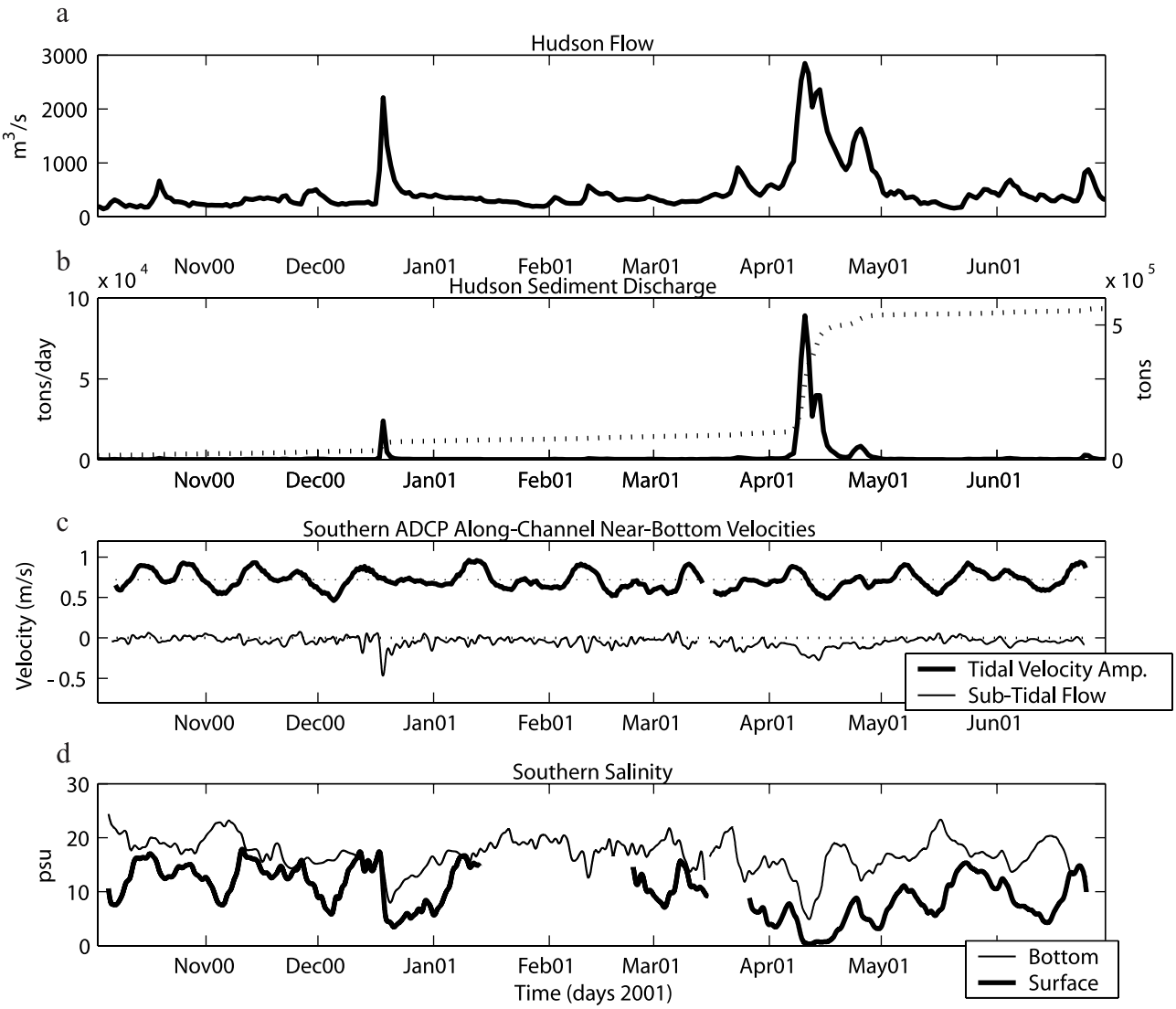

Figure 4. Time series of forcing conditions in the Hudson estuary during the field study. (a) Hudson water discharge from the sum of the Hudson discharge measured at Waterford, New York, and Mohawk River discharge measured at Cohoes, New York. (b) Hudson sediment discharge estimated using a rating curve from *Woodruff et al.* [2001] and cumulative discharge (dotted line, right *y* axis). (c) Near-bed (1.5 mab) tidal velocity amplitudes and mean velocity at the southern depositional site. (d) Low-pass-filtered salinity from the southern depositional site tripod (near-bottom) and surface buoy. Date tick marks are located on the first of the month.

share the common characteristic of a rapidly decreasing settling velocity near C_{gel}.

3.3. Shipboard Sampling

[15] Shipboard measurements were conducted at four times during the tripod deployment: in October (deployment), March (turnaround), April (freshet), and June (recovery). During the April observations, conductivity-temperature-depth (CTD) and OBS casts were performed both in across- and along-channel transects as well as hourly casts at a single site (near the southern central tripod) over a complete tidal cycle. Each CTD cast also had a Niskin bottle, which was opened 30 cm above the bed to collect a suspended sediment sample for use in calibrating the OBS and ABS sensors.

[16] During deployment, turnaround, and recovery an extensive set of cores were taken to examine the changes in seabed structure over a seasonal timescale. Three types of coring techniques were employed. Box cores and hydraulically damped piston (referred to as "slow") cores were taken near the tripod sites and at a series of stations that have been cored extensively since 1998 [*Woodruff et al.*, 2001]. Scuba divers took push cores directly under the tripod at recovery. The cores were X-radiographed to examine fine vertical scale sedimentary stratigraphy. Cores were also photographed to document vertical structure of mud color, which indicates the state of oxidation. Resistivity measurements were taken on the slow cores to estimate vertical profiles of porosity. Slow cores retrieve a relatively undisturbed sediment-water interface and thus are ideal for

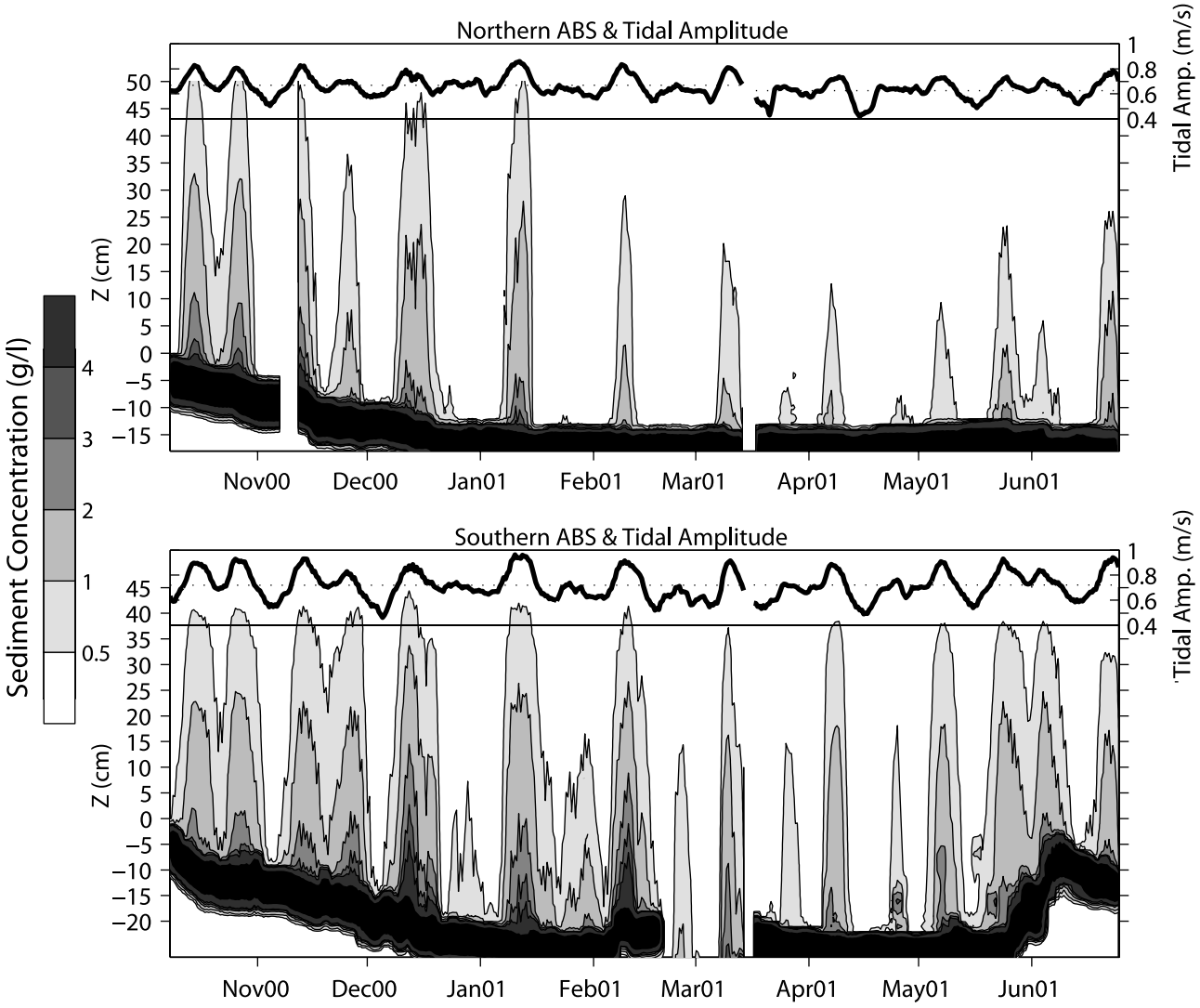

Figure 5. Low-pass-filtered ABS sediment concentration profiles and bed elevation time series from the northern and southern convergence sites. The thick black trace represents scattering from the bed. Low-pass-filtered tidal amplitude is also plotted at the top of each panel for both sites. The low-pass filter used to process these data averaged the period from 4 to 6 hours and from 8 to 10 hours after slack low water to estimate maximum velocity and concentration during flood and ebb, respectively.

examining high-porosity, recently deposited sediments. Radionuclide measurements were also performed on the cores to quantify the scales of deposition [*Sommerfield*, 2003].

4. Results

4.1. Seasonal Variations

[17] The Hudson River flow was marked by two freshet events during the observational period (Figure 4). A relatively small event occurred in December, delivering ~100,000 t based on the rating curve of *Woodruff et al.* [2001]. The second, more significant freshet occurred in April and delivered an estimated 500,000 t of new sediment to the estuary. Thus the total amount of new sediment introduced into the estuary is ~600,000 t, which is slightly more than the average yearly load of 400,000 t [*Woodruff et al.*, 2001]. The freshet events produced brief periods of strong southward net flow, but throughout the deployment the velocities were dominated by tides, which showed a strong spring neap modulation. These freshet events can also be seen in the salinity record, which shows entirely fresh water at the surface and 5–7 psu at the bottom during the second freshet.

4.1.1. Bed Elevation Data

[18] Bed elevation data show dramatic changes through the seasonal timescale at both the northern and southern tripods (Figure 5). Both sites show erosion for the first 3 months of the deployment. The southern site bed elevation decreases by 20 cm from October to January. During this same period the northern site decreases elevation by 13 cm. The southern site tripod was knocked over in late February, as indicted by tilt sensor changes of 20° and dents in the tripod frame. The tripod was redeployed in mid-March in the correct vertical orientation. An apparent deposition event at the southern site in mid-February should be interpreted with caution as the tripod began to tilt shortly after this event.

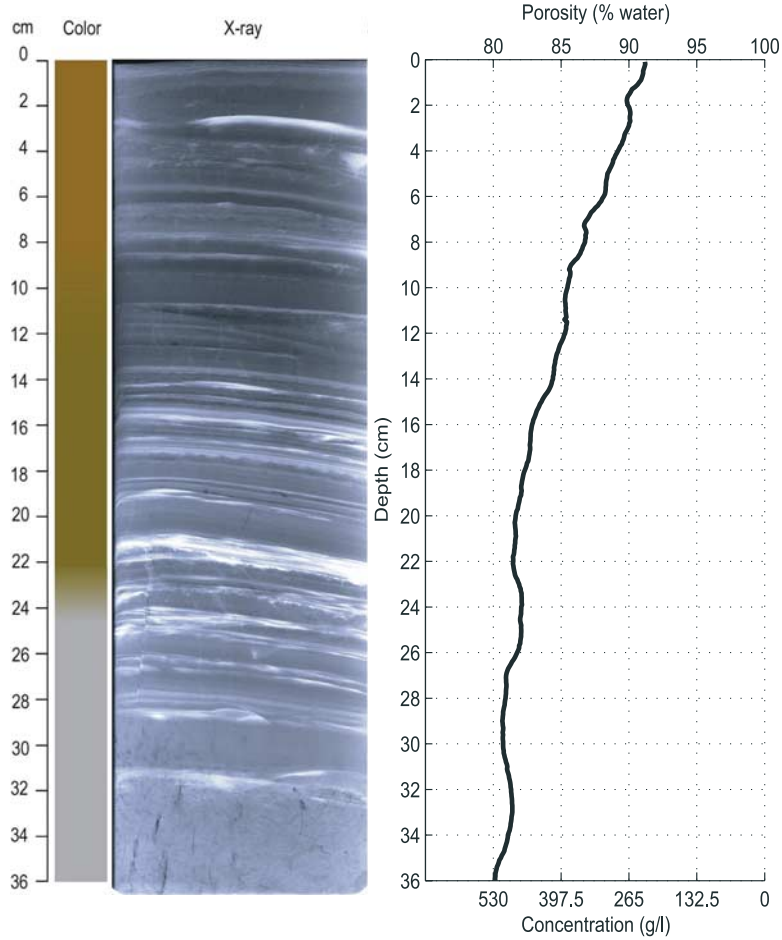

Figure 6. (left) An X-radiograph negative and photo color from a box core taken ~30 m from the southern tripod 2 days after the end of the deployment in June. Light areas in the X-radiograph are higher-density very fine sand and silt layers, and dark areas are clay and silt. (right) Porosity profile from resistivity measurements from the same box core.

[19] The sediment cores taken in October 2000, January 2001, March 2001, and June 2002 were compared, using distinctive marker beds, to provide an alternative measure of net erosion and deposition [*Sommerfield*, 2003]. These measurements show ~8–11 cm of erosion at the sites between January 2000 and March 2001. During the same period the ABS data at the southern site show nearly twice as much erosion and 2 cm more erosion at the northern site than the core data. The additional erosion detected by the ABS is likely the result of enhanced scour due to the flow distortion by the tripods themselves. A potential flow analysis indicates an increase in velocity of about 5% at the bed due to the flow around the pressure cases on the tripods, which may be enough to explain the initial scour. On the basis of the sediment core data, it appears that significant erosion did not occur until after the January cores were taken. This is inconsistent with the ABS data, which show erosion occurring earlier, again suggesting enhanced initial erosion under the tripods.

[20] At the southern site the ABS data show a depositional event of 20 cm beginning in late May and continuing through mid-June. This depositional event occurs 1.5 months after the April freshet, during spring tide conditions. Some of this sediment is eroded away in late June, leaving a net deposit of 13 cm under the tripod. The northern site shows 1 cm or less deposition during this same period. The core data from June 2002 show 24 cm of deposition (brown sediment in Figure 6) at a site 30 m from the tripod. A separate core, taken by divers within 1 m of the tripod, shows 19 cm of deposition. Cores taken at the northern site show no deposition during this period. The favorable comparison with the core data suggests that the ABS measurements of sediment deposition are reliable.

4.1.2. Suspended Sediment Data

[21] Suspended sediment data from the southern site are presented in Figure 7 and were calculated using a tidally phase-coherent filter that averages the concentration in the lower 30 cm of the water column from 2 to 4 hours and 8 to 10 hours after low slack water. Flood and ebb estimates are plotted separately. This effectively provides an estimate of the maximum sediment concentration resuspended in flood and ebb tidal phases. To further reduce variability for displaying, the data for flood and ebb were averaged with a three-tidal cycle running average filter. Velocity data from the lowest ADCP bin at 2.5 m above the bed were processed in a similar manner. Since deposition occurred only at the southern site, all data discussed henceforth are from the southern site unless otherwise noted.

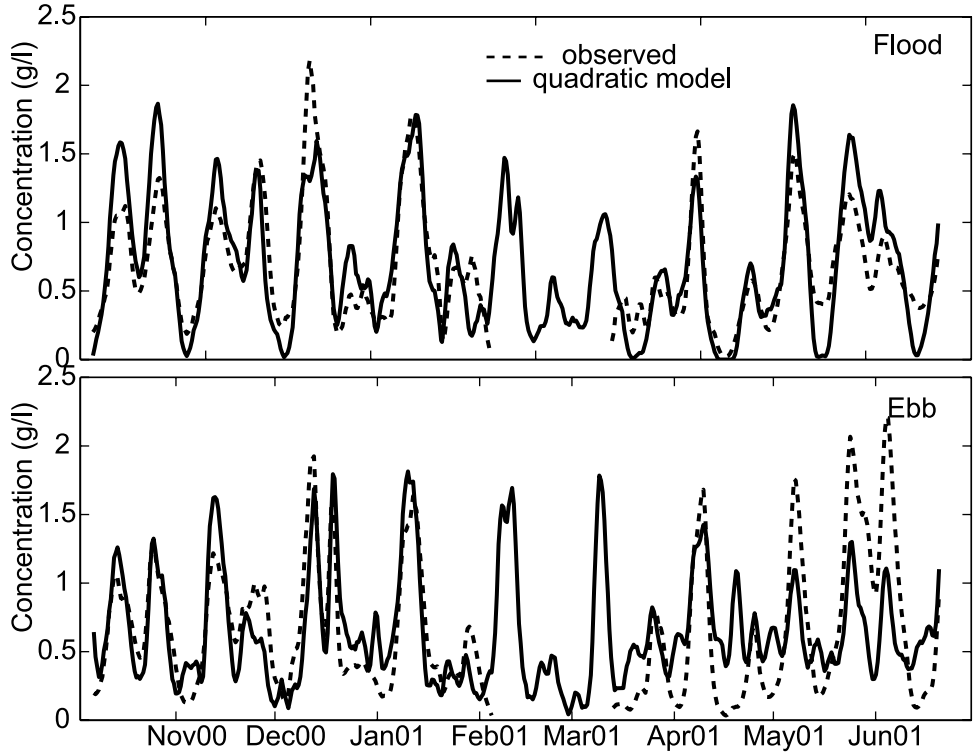

Figure 7. Time series of sediment concentration depth averaged over the lower 30 cm estimated from the ABS sensor (dashed lines) and quadratic model (equation (2), solid lines). The temporal filter used to process these data averaged the period from 4 to 6 hours after slack low water to estimate maximum velocity and concentration during flood and the period from 8 to 10 hours after slack low water to estimate maximum velocity and concentration during ebb. The observed concentration significantly exceeds the model during ebb spring tides in May and June, suggesting trapping during those periods.

[22] The dominant signal of the filtered suspended sediment data is the fortnightly variation with tidal amplitude. Concentrations are <0.5 g L^{-1} during neap tides and >4 g L^{-1} during spring tides at the southern site. The spring tide concentrations at the northern site were not as high, reaching 2 g L^{-1}. There was no particular evidence in the suspended sediment record of the April freshet, even though it is believed that most of the sediment input to the estuary occurred at that time. This indicates the dominant influence of tidal resuspension in determining the suspended sediment concentrations.

[23] The near-bottom concentration (C depth averaged over the lower 30 cm with units of g L^{-1}) variations were significantly correlated with near-bottom velocity (U) for most of the deployment. Two different approaches yield roughly similar correlations. A power law of the form

$$C = C_0 U^5$$

was found to yield a regression coefficient (R^2) of 0.89 from the beginning of the deployment until mid-May. A quadratic form with a critical erosion velocity,

$$\begin{aligned} C &= C_0 \frac{(U^2 - U_c^2)}{U_c^2} \quad U \geq U_c \\ C &= 0 \qquad\qquad\quad U < U_c, \end{aligned} \tag{2}$$

yielded correlations of 0.87 for all flood tides and 0.76 for ebb tides before May 2001. Here the critical velocity for resuspension U_c = 56 cm s^{-1} and C_0 = 0.88 g L^{-1}. The latter formulation is consistent with a *Partheniades* [1965] erosion law, although the erosion threshold is surprisingly high for a fine-sediment environment. In Figure 7, it can be seen that this model is generally able to predict the sediment concentration, with the most noticeable exception being the period during late May and June on ebb. During this period the sediment concentration is high relative to the velocity. On the basis of previous studies [*Geyer et al.*, 1998] that suggest trapping should occur on the western shoals during ebb, these data suggest that the high ebb concentrations relative to the velocity are likely the result of sediment trapping. It is noticeable that significant trapping only occurs at the end of the deployment, 1–2 months after the spring freshet.

[24] During this period of enhanced trapping in May and June 2001, there were episodes of very high near-bottom concentrations at the southern site (Figure 5), resembling short-term changes in bottom elevation. These were determined to be due to fluid mud (i.e., suspended sediment concentrations in excess of 10 g L^{-1}), and they will be discussed in more detail in section 4.2.

4.2. Tidal Variations During the Depositional Interval

4.2.1. Bed Elevation Data

[25] To demonstrate the sequence of events that produce the deposition in early June, three spring neap cycles bracketing the depositional period in May and June are shown in Figure 8. During the spring tide in early May (the

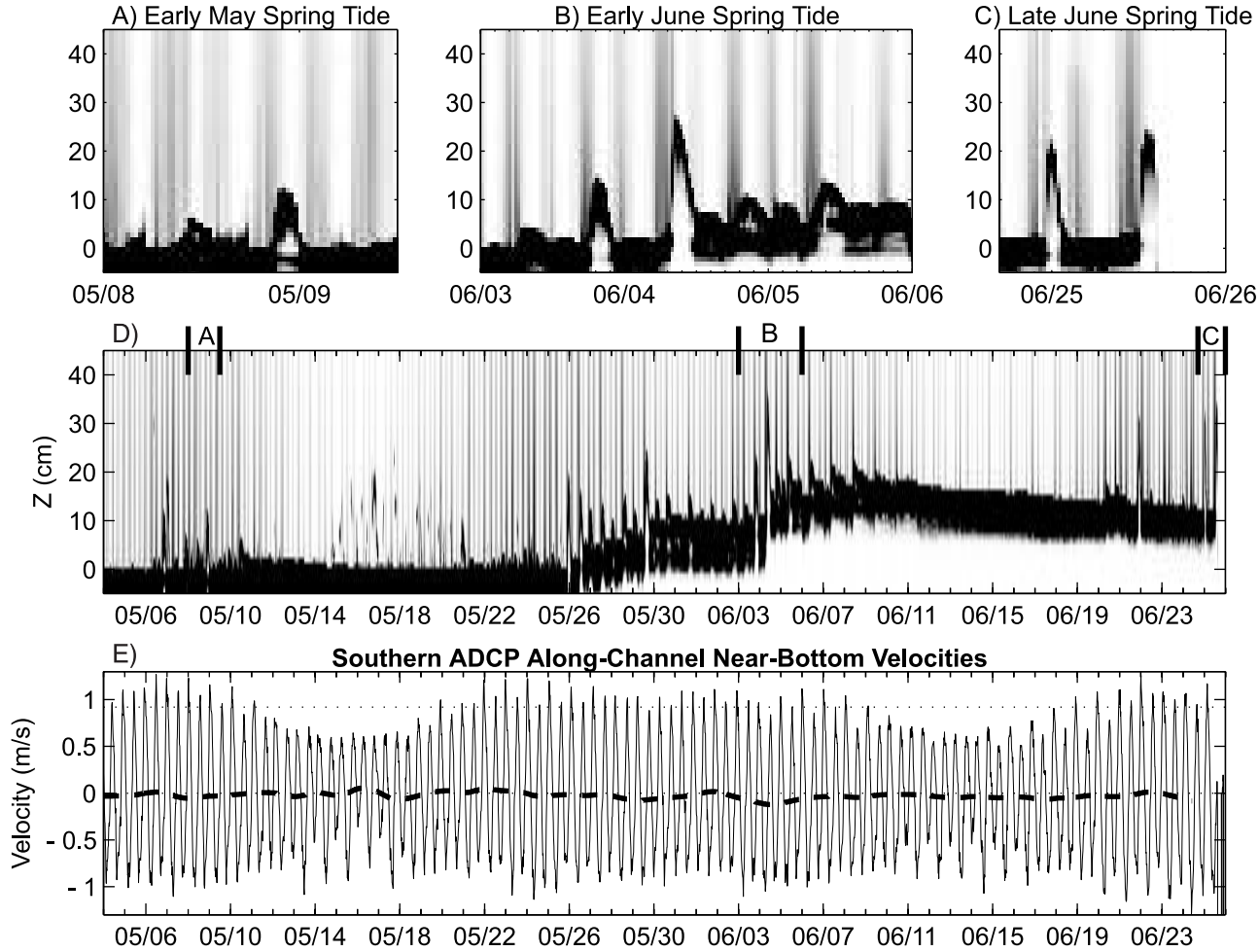

Figure 8. (a–c) Three periods of ABS data showing transient fluid mud deposits as delineated by regions labeled A, B, and C in Figure 8d. (e) ADCP data from 2.5 mab with low-pass-filtered data (dashed line).

second spring tide after the April freshet), 10–15 cm changes in apparent bottom elevation are visible on a tidal timescale. During these elevation changes, there is acoustic scattering from both the new scattering layer and from the original bed at a lower intensity. The penetration of the acoustic signal through this new layer is consistent with the laboratory settling tank experiments for thin layers of recently settled mud (concentrations of 150–250 g L^{-1}). The transient deposits during the spring tide in early May are not associated with net changes in bottom elevation, in contrast to the later observations.

[26] In late May and early June, there are larger bed elevation changes at the tidal timescale, with maximum amplitude of 24 cm on 4 June. Unlike the events in early May, these transient deposits leave a substantial deposit, with an accumulated elevation change of +18 cm from 26 May to 9 June. Several individual semidiurnal tidal cycle events during spring tides leave 1–3 cm deposits, which, in aggregate, produce the large net gain in bed elevation. These transient deposits also have a different acoustic signature than those of the previous spring tide as the acoustic return from the original seabed completely disappears. This is consistent with observations in the laboratory settling tank experiments when the thickness of the new deposits exceeds 10–15 cm.

[27] These transient deposit events all begin occurring on the tidal cycle following the highest velocity cycle of that spring tide. The transient deposits do not occur during neap tides. However, there is a neap tide period (14–20 May), in which there are several episodes of a thin (1–2 cm) layer of high acoustic backscatter 10–20 cm above the bed. These events are not associated with high suspended sediment concentrations as the backscattered intensity is low, except at the thin layer, and the acoustic return from the bed is not reduced as it is during the depositional events. In the 1 Hz burst data, these high scattering layers show small-scale internal waves, and discrete scatters were not visible. Our current hypothesis is that these signals represent scattering from the density interface associated with high-salinity layers that sometimes appear near the bed during neap tides. Throughout the ABS data the high correlation with hydrodynamic forcing and the high sediment concentrations indicates scattering from biological scatters is most likely low relative to scattering from sediment.

4.2.2. Suspended Sediment and Hydrodynamic Forcing During Deposition Events

[28] The relationship between sediment concentration, bed elevation, and hydrodynamics during the early June depositional event are illustrated in Figure 9. The suspended sediment reaches its maximum concentration (2–4 g L^{-1})

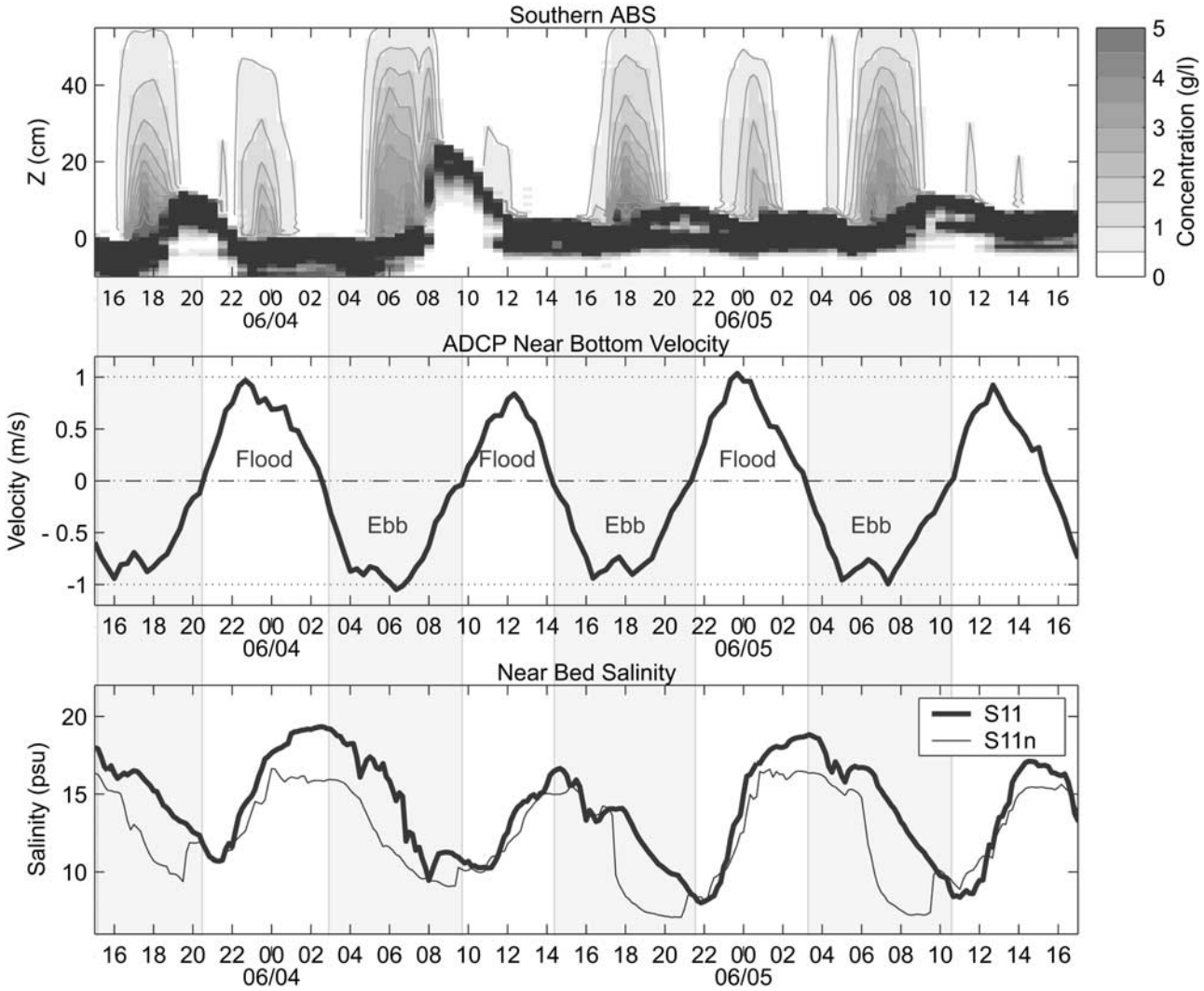

Figure 9. (top) Four tidal cycles of ABS data showing transient deposits of fluid mud. Contours of sediment concentration are spaced 0.5 g L^{-1} apart. (middle) Acoustic Doppler current profiler (ADCP) tidal velocity from 2.5 mab. (bottom) Salinity from the southern depositional site tripod (S11) and the small tripod located 500 m to the north (S11n).

close to maximum ebb. As the concentration decreases during the waning ebb, the bottom elevation rapidly increases. The transient deposit begins to thin during the early flood before there is appreciable resuspension. Flood resuspension reaches its maximum close to the time of maximum flood current, but the concentrations are less than half of those during the ebb, even though the velocities are similar.

[29] The large difference between ebb and flood concentrations for similar velocities (Figure 7) suggests that horizontal trapping processes may be important during the ebb, thus augmenting the supply of sediment relative to that due to local resuspension. The salinity difference between the southern depositional site (S11) and the tripod located 1 km to the north (S11n) reaches as much as 5 psu during the ebb (Figure 9 (bottom)), indicating strong frontal conditions. The average salinity gradient in the estuary is about 1/10th this value. The influence of this front on the velocity at the southern depositional site is evident in the reduction in velocity close to the time of maximum ebb (Figure 9 (middle)). The presence of this front causes a near-bottom velocity reduction on the order of 30 cm s^{-1} relative to the barotropic tidal flow, which is approximately sinusoidal [*Geyer et al.*, 2000]. This velocity reduction is associated with a near-bottom convergence across the front that results in the convergence of suspended sediment flux and high ebb concentrations.

4.3. Intratidal Processes

[30] To gain further insights into the processes that are creating these transient fluid mud deposits, the 1 Hz, burst-sampled ABS data were examined for the tidal cycle in which the largest net elevation changes were observed. In Figure 10, three intervals of 10 min, 1 Hz sampled bursts of ABS data are shown with the burst-averaged ABS and velocity data for the corresponding tidal cycle on 4 June. Several phases of bed evolution are evident. In the first phase, high suspended concentrations occur during maximum ebb, when frontal trapping is strongest. The bed

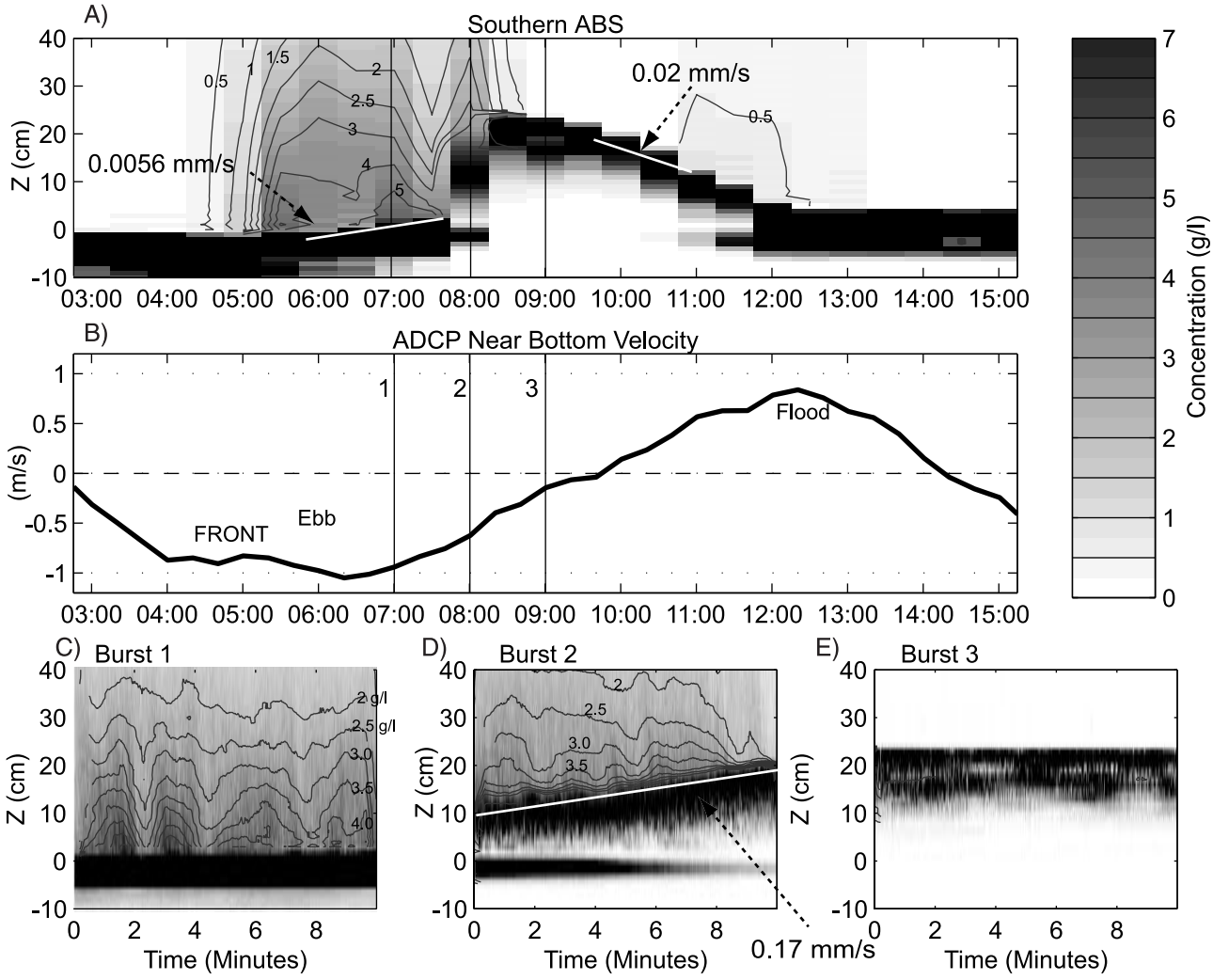

Figure 10. (a) Burst-averaged half hourly sampled ABS data from 4 June. Contours of sediment concentration are spaced 0.5 g L^{-1} apart. (b) ADCP tidal velocity 2.5 mab. (c–e) Three bursts of 1 Hz sampled ABS data at times 1, 2, and 3, as indicated in Figures 10a and 10b. Figure 10c shows a turbulent suspension. Figure 10d shows the rising mud-water interface as sediment deposits, and Figure 10e shows some internal acoustic structure in the recent deposit.

elevation slowly rises at ~2 cm h^{-1} (0.0056 mm s^{-1}). During waning ebb (0800 LT) the bed rises at an extremely rapid rate of 1 cm min^{-1} (0.17 mm s^{-1}), based on the burst-sampled data. There is high backscatter from the mud-water interface, and backscatter is visible from the original seafloor below the fluid mud layer. In the burst-averaged plot the interface appears diffuse at this time due to averaging over an interface that is moving rapidly upward. The concentrations immediately above the bed are 4–6 g L^{-1} during this period of rapid elevation change.

[31] As the tidal velocities decrease in transition to flood, the near-bed suspended concentrations decrease to 0.4–0.6 g L^{-1}, and bed elevation begins to decrease slowly. At the beginning of flood the suspended concentrations are low (<0.3 g L^{-1}), and the bed elevation decreases at ~8 cm h^{-1} (0.02 mm s^{-1}). Suspended concentrations increase to 1 g L^{-1} 1 hour before the flood velocity maximum, during which the bed elevation continues to decrease at the same rate as in the early flood. The decrease in elevation of the bed during the early flood appears to be due to consolidation of the fluid mud layer, although erosion probably becomes significant during the strong flood tide.

4.3.1. Laser In-Situ Scattering and Transmissometry (LISST) Data

[32] Information about the suspended sediment size distribution 1.5 m above the bed was available from the LISST sensor (Figure 11). A representative time series of LISST data was phase averaged over eight tidal cycles starting on 17 March 2001 during neap tide. Phase averaging was performed using the velocity zero crossing before flood as a time reference so that each point in the phase-averaged result represents the mean value averaged over multiple tidal cycles at the indicated time after the start of flood. The concentrations during spring tides were too high for the sensor to function properly (transmission over the 2.5 cm path was reduced to below 30% of full scale). In both ebb and flood, before maximum velocity the particle diameters were between 25 and 125 μm, with means around 30–50 μm.

During flood, as maximum velocity was reached, the suspended particles became slightly smaller, while during ebb, the particle size first became larger then slightly smaller with increasing velocity. On both flood and ebb just after maximum velocity the particle size becomes significantly larger, presumably due to flocculation, and then rapidly settles out of suspension. The mean diameter increases almost an order of magnitude, from 40 to 250 μm, before the rapid settling.

4.3.2. Sediment Core Data

[33] Sediment cores obtained at the end of the deployment provide a record of the thickness and internal bedding characteristics of the transient mud deposits. In the late June spring tide, at the very end of the deployment, a 20-cm-thick transient deposit was emplaced. In fact, the tripod recovery operation took place when one of the transient deposits was present (Figure 8c). A scuba diver took push cores under and immediately adjacent to the tripod shortly before the ABS record ends on 25 June. An X-radiograph (Figure 12) of the core adjacent to the tripod shows a recently deposited homogeneous mud bed in the upper 4 cm. Below this are several centimeters of internally laminated beds of very fine sand and silt (4.5–10 cm thick) and then another homogenous mud (clayey silt) bed. The grain size distributions from these beds show the very fine sand and silt laminae to have mean grain sizes of ~15 μm, while the mud beds have mean grain sizes closer to 10 μm. Unfortunately, no porosity data were available from this core.

[34] A resistivity-porosity profile measured on a box core collected 2 days later (Figure 6) does not show a recently deposited mud layer. This core appears to have a very fine sand and silt layer at the surface, perhaps as a product of erosion and winnowing of a previously emplaced transient tidal deposit. The porosity values in the surface layer are in the low 90% range and decrease with depth to 80–85% at depths of 10–20 cm. Sediment color is also shown from the same box core (Figure 6 (left)), revealing 22 cm of brown (i.e., oxidized) sediment at the surface, which is associated with recent deposition [*Woodruff et al.*, 2001]. This is approximately consistent with the ABS seasonal deposition of 18 cm. As mentioned in section 4.2.1, flow disturbance near the tripod may make the tripod location slightly more erosive than adjacent areas; thus it is not surprising that the box core shows slightly more seasonal deposition than the ABS elevation data.

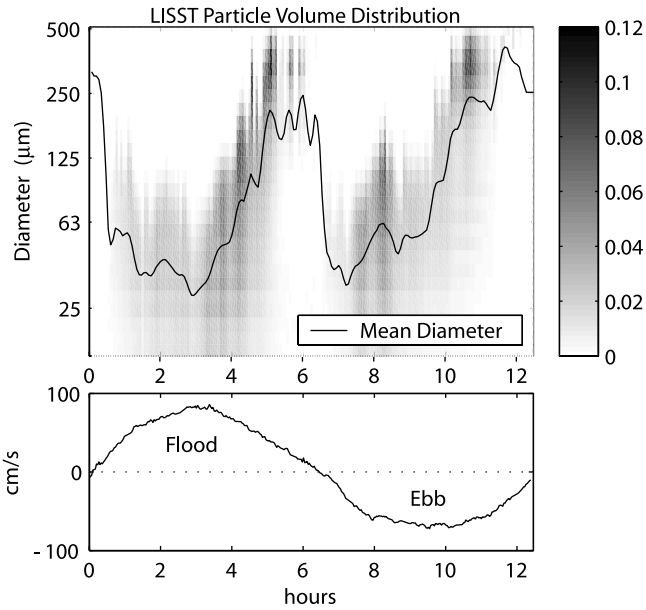

Figure 11. (top) Phase-averaged particle volume distributions (volume per size class) from a Laser In-Situ Scattering and Transmissometry (LISST) sensor located 1.5 mab at the southern site. The gray intensity scale is normalized so that the distribution with most volume, just after 4 hours, integrates to unity. The line is the mean diameter as a function of tidal phase time. (bottom) Phase-averaged velocity. In both plots, phase averages were performed over eight tidal cycles during neap tide starting on 17 March 2001.

5. Discussion

5.1. Trapping Processes

[35] The trapping of sediment occurs at three vertical scales: first, there is the horizontal convergence of suspended sediment within the water column that results in enhanced concentrations during the ebb; second is the settling of suspended sediment into a transient layer of fluid mud; and third is the consolidation of the fluid mud into the formation of new bed material. The accumulation of bed sediment in the ETM appears to be the result of the sequential occurrence of all three of these trapping processes. An interpretation of the trapping mechanisms at each of these vertical scales is treated in sections 5.1.1–5.1.3.

5.1.1. Frontal Trapping of Suspended Sediment

[36] Through most of the annual cycle, tidal resuspension dominates the suspended sediment signal, and similar concentrations are observed during ebb and flood (Figure 7). In late May, when significant depositional events are observed, an asymmetry is observed between flood and ebb conditions. Whereas the relationship between suspended sediment concentrations and the quadratic velocity resuspension model during flood remain the same during this period, the ebb concentrations increase by nearly a factor of 2 relative to the velocity model. The observations and model studies of *Geyer et al.* [1998] indicate that sediment trapping occurs during ebb in association with the development of a front and the associated near-bottom convergence of sediment. This is clearly the case in this study: the intensity of the salinity gradient just to the north of the southern site reaches 5 psu km^{-1} during the ebb, ~10 times the average estuarine salinity gradient. The convergence of sediment flux results from the enhanced vertical velocity in the convergence zone where the ebb flow encounters the front [*Geyer*, 1993]. The magnitude of the vertical velocity could not be accurately estimated from the tripod array, but the horizontal convergence of velocity was evident in the measurements from the advection of the velocity deficit during ebb (Figure 9 (middle)). Although the water column convergence of sediment could not be tested quantitatively, the suspended sediment, velocity, and salinity data all provide a consistent indication of frontal convergence in the classical sense of the estuarine turbidity maximum [*Postma*, 1967].

[37] Observations during April 2001 illustrate the frontal conditions that lead to sediment trapping (Figure 13). During the flood, sediment is transported northward in the

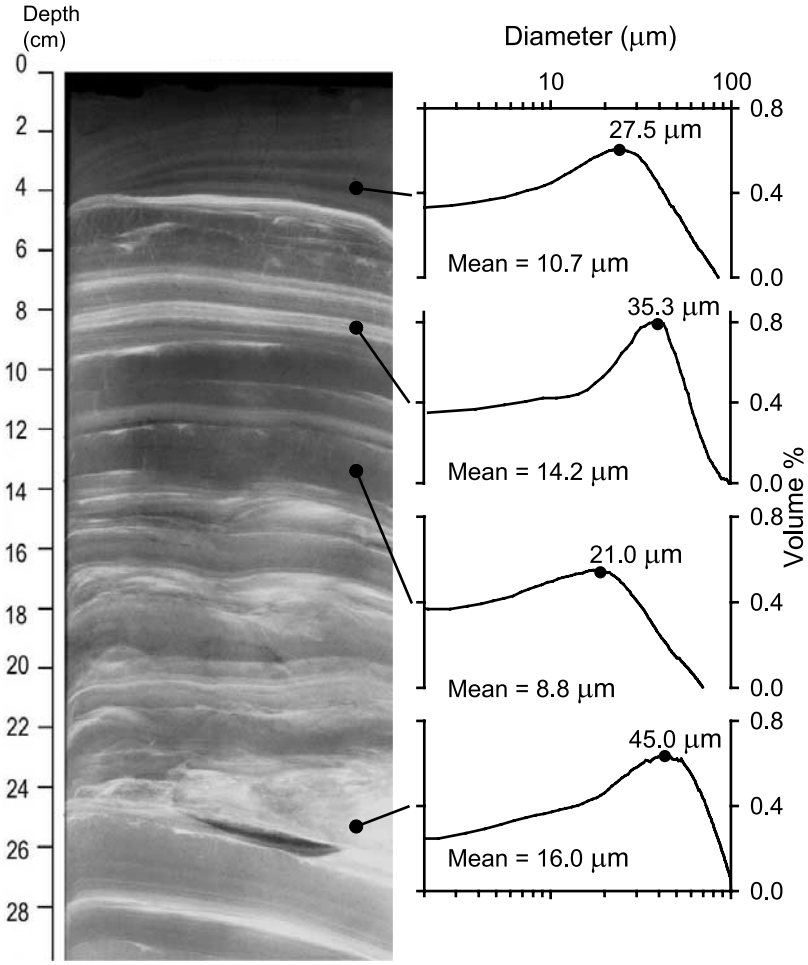

Figure 12. (left) An X-radiograph negative from a core taken by divers adjacent to the southern tripod at the end of the deployment on 25 June. Light areas are higher-density sand and silt layers, and dark areas are mud. (right) Grain size distributions for coarser and finer grain size laminae within the bed. Mean and mode grain sizes are shown for each distribution.

eastern channel, where the highest salinities and highest velocities occur. Secondary circulation induced by the cross-channel density gradient causes westward transport at the end of the flood (also indicated in the model simulations by *Geyer et al.* [1998]) so that the highest concentrations during the ebb occur on the shallower west side. During the ebb, frontal conditions develop just upstream of S11, and sediment advected from the north settles downstream of the salinity front due to the combined influence of the convergence of bottom velocity and the reduction in shear stress downstream of the front. Although the salinity was lower in April than during the depositional period in late May (Figure 4d), the horizontal salinity gradient was similar (based on time series measurements of the advection of the horizontal gradient), so it is inferred that the frontal structure is similar in the May and June trapping periods.

[38] An unresolved question in this study is why the intense trapping occurred at the southern depositional site not during the freshet when new sediment entered the system but 1–2 months later. This delay in sediment deposition was also observed in the Hudson estuary by *Woodruff et al.* [2001], who suggest that the northward transport of sediment following the freshet provides the supply for the observed trapping in the ETM. The northward flux of sediment following the freshet was clearly documented by water column measurements [*Geyer et al.*, 2001] and by geochemical studies [*Feng et al.*, 1999].

[39] The observations in this study (Figure 13) indicate that strong frontal conditions occur during the freshet, which would be expected to result in sediment trapping if there were an adequate supply of sediment. It appears, however, that there was not an adequate sediment supply in the bottom boundary layer during the freshet. The incoming sediment may have been more dispersed through the water column due in part to the lack of stratification to the north during freshet conditions and possibly due to less particle aggregation within the fresh water. The measured concentrations during this period of southward flux are not exceptionally high (Figure 7), but there could still be a large southward flux due to the mean southward flow and the extended duration of the freshet (Figure 4). The sediment may also have been transported seaward primarily in the deeper eastern channel during the freshet. The observations by *Geyer et al.* [2001] of the relatively modest 1999 freshet indicate net southward transport only during the freshet

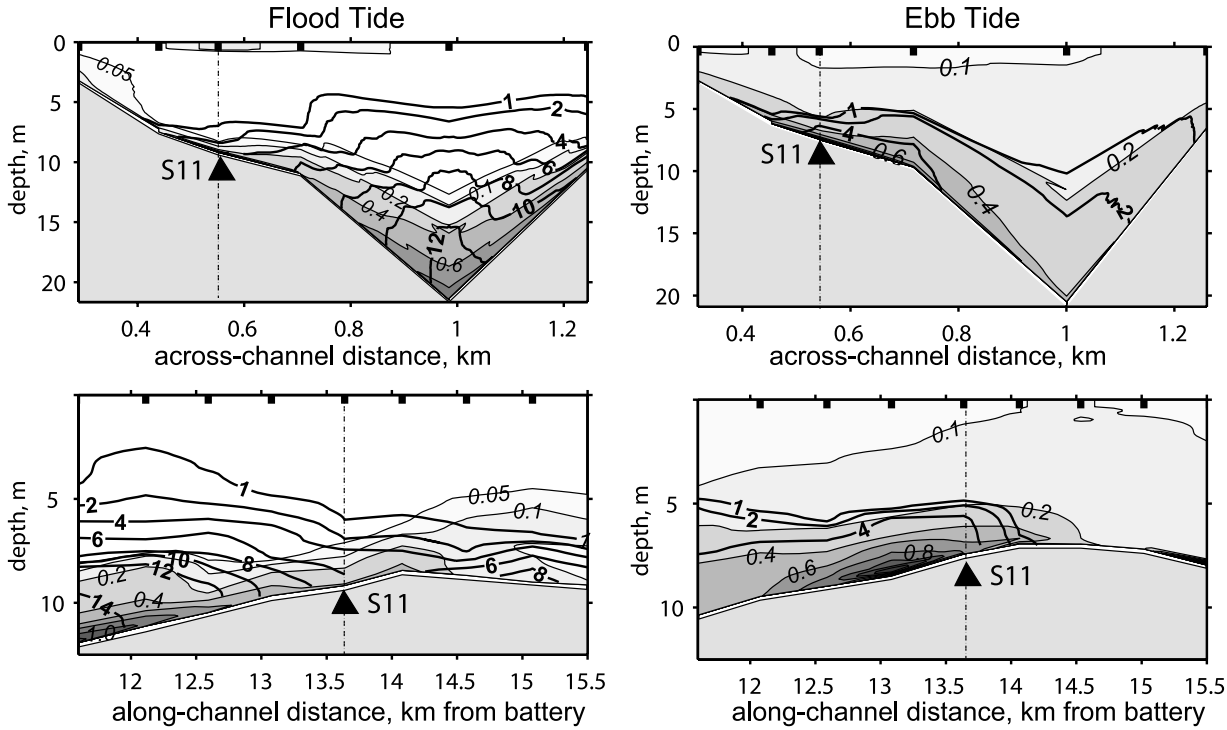

Figure 13. (top) Across- and (bottom) along-channel distributions of salinity (thick solid line contours with units of psu) and OBS sediment concentration (filled contours with units of g L^{-1}) data during (right) ebb and (left) flood, showing frontal trapping conditions during mid-April. Station locations are indicated by thick black ticks in the upper part of the plot, and the southern tripod site (S11) is shown as a filled triangle. The highest concentrations during ebb are just downstream of the maximum salinity gradient on the western shoals. During flood the sediment concentration is highest in the eastern channel and south of the study site.

period, followed by strong northward flux. Also, the sediment cores of *Woodruff et al.* [2001] indicate that sediment is trapped in the southern part of the estuary during the freshet and is remobilized and transported northward over 1–2 months following the freshet. This result is also consistent with the geochemical evidence of *Feng et al.* [1999] that sediment trapped within the mid-estuary turbidity maximum zone is transported from a region of higher salinity.

[40] Only after the freshet, when sediment was most likely remobilized from farther south in the estuary, did near-bottom concentrations on the western shoals become adequate to cause significant sediment trapping and deposition. There could also be a temporal dependence to the trapping in that several spring tidal cycles with strong frontal convergence and adequate sediment supply are required to create high enough concentrations to lead to the observed deposition. *Dyer* [1978], in an analysis of horizontal flux terms in several estuaries, noted that the position of the ETM may respond more slowly to the changing estuarine dynamics than to the salt distribution due to the time required to move sediment.

[41] Flux measurements from *Geyer et al.* [1998] and depositional mass estimates at the southern depositional site from *Woodruff et al.* [2001] can be used to examine the temporal lag observed in this study. While this study did not measure channel-integrated flux as we did not have a mooring in the deeper eastern channel, *Geyer et al.* [1998] estimated that each spring tide carried 50,000–80,000 t of sediment northward past lower Manhattan. *Woodruff et al.* [2001] estimate that the depositional sites north and south of the George Washington Bridge contained 300,000 t of new sediment with approximately half of the sediment in each area. On the basis of this flux rate and depositional mass, it would take at least two spring tides to transport sufficient sediment northward to form the observed deposit. This is consistent with the results of our observations, which indicate that deposition occurred at the southern site on the third spring tide after the April freshet.

5.1.2. Formation of Transient Mud Deposits

[42] A simple explanation for the formation of the transient deposits would be the local settling of suspended sediment during the late ebb. The suspended sediment in the water column during the peak of ebb flow would produce a 3–6 cm transient deposit based on an estimated porosity of a fluid mud layer of 98% (thin solid line in Figure 14). However, the transient deposits are 15–25 cm thick, indicating that there must be a significant convergence of sediment flux during ebb.

[43] This sediment convergence process is associated with the frontal hydrodynamic convergence that leads to the enhanced suspended sediment concentrations, resulting in an excess of suspended sediment downstream of the front, which settles at a rate greater than the local rate of resuspension. Deposition of sediment would occur just due to the excess suspended sediment at the front, even if the

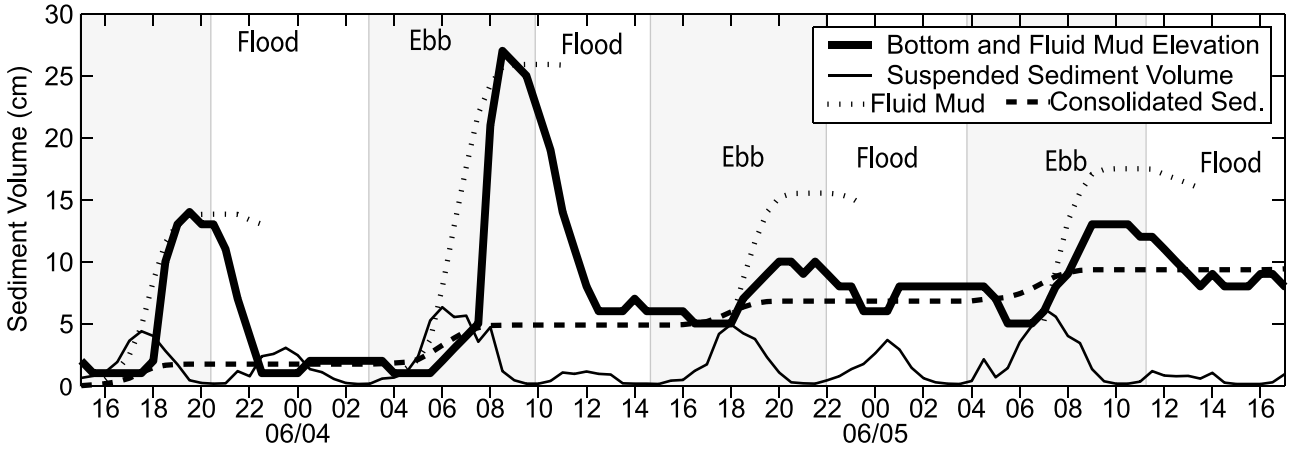

Figure 14. ABS measured bed elevation (thick solid line) and models for bed elevation changes. The depth-integrated volume of sediment in suspension (thin solid line with units of $cm^3\ cm^{-2}$ and based on an assumed porosity of 98%) is not able to predict the bed elevation changes, indicating that convergence is required. The discontinuous dotted line is from the convergence model (equation (3)) based on a porosity of 98% for the accumulation of transient deposits of fluid mud. This is only plotted during the depositional period of ebb and into early flood since the convergence model does not account for the rate of consolidation. The dashed line is from the convergence model (equation (3)) based on a porosity of 80% for the accumulation of consolidated mud over a longer timescale.

bottom stress remained constant. However, this deposition process is greatly enhanced by the reduction in stress behind the front due to the reduction in near-bottom velocity. If the reduction of stress is great enough that the stress falls below the threshold for resuspension, then virtually the entire layer of sediment is trapped behind the front.

[44] A model for the convergence process can be based on the assumption that the convergence in water column flux balances the vertical growth of the transient layer:

$$\frac{dQ}{dx} = (1-p)\frac{d\eta}{dt}, \tag{3}$$

where Q is the vertically integrated sediment flux, η is the elevation of the transient deposit, and p is the porosity, assumed to be constant throughout the layer. The horizontal scale of convergence is determined in part by the scale of the salinity front, which determines the scale over which the stress reduction occurs. The trapping scale is also controlled by the settling rate of sediment according to the relation

$$x_s = \delta(u_b/w_s), \tag{4}$$

where x_s is the horizontal scale of sediment settling out of the boundary layer, δ is the boundary layer thickness, u_b is the near-bottom velocity, and w_s is the settling velocity of the sediment. With values of δ = 1 m, u_b = 50 cm s^{-1}, and w_s = 1 mm s^{-1}, the trapping scale is 500 m. This is also on the order of the horizontal scale of the front, so it represents a reasonable estimate of the convergence scale (dx in equation (3)).

[45] To estimate flux convergence, the depth-integrated ABS data are used with the assumption that flux goes to zero at the horizontal convergence scale (x_s). This deposition estimate based on flux convergence with an assumed porosity of 98% is able to approximately predict the magnitude of the transient fluid mud deposits for each ebb tidal phase (dotted line in Figure 14). Once this high-porosity deposit is put in place, it will dewater, consolidate, and potentially erode during flood. The observed accretion rate can be produced by the estimated flux convergence rate if the porosity is assumed to be 80% (dashed line in Figure 14). However, resistivity measurements indicate that the porosity averaged over the upper 20 cm is 85%, suggesting that about one fourth of the recently deposited sediment is eroded during flood tides and that the remaining decrease in the thickness of the layer is due to consolidation and dewatering.

[46] Figure 14 also shows that the recently deposited layers decrease in thickness by a factor of ~4 due to consolidation and erosion during late ebb and flood tidal cycles. Given that the near-surface porosities were measured in the low 90s after the consolidation of the fluid mud layer, if we use the estimate that most of the decrease in thickness is due to consolidation, this suggests that the mud beds are deposited at porosities in the high 90s. This is consistent with the assumption of 98% used to predict the thickness of the transient deposits from flux convergence.

[47] To further examine the consistency of the hypothesis that the transient deposits are formed by the settling of suspended sediment, which is supplied by flux convergence, we can examine the short-term accumulation rates relative to settling depositional flux. The ABS data (Figure 10d) show that sediment can accumulate at rates as fast as 0.17 mm s^{-1} to form the transient deposits. The depositional flux required to create this accumulation rate is equal to the concentration times the settling velocity. The concentration is known from the ABS data, and settling velocities can be estimated from the hindered settling curve based on the laboratory settling experiment (equation (1) as plotted in Figure 15).

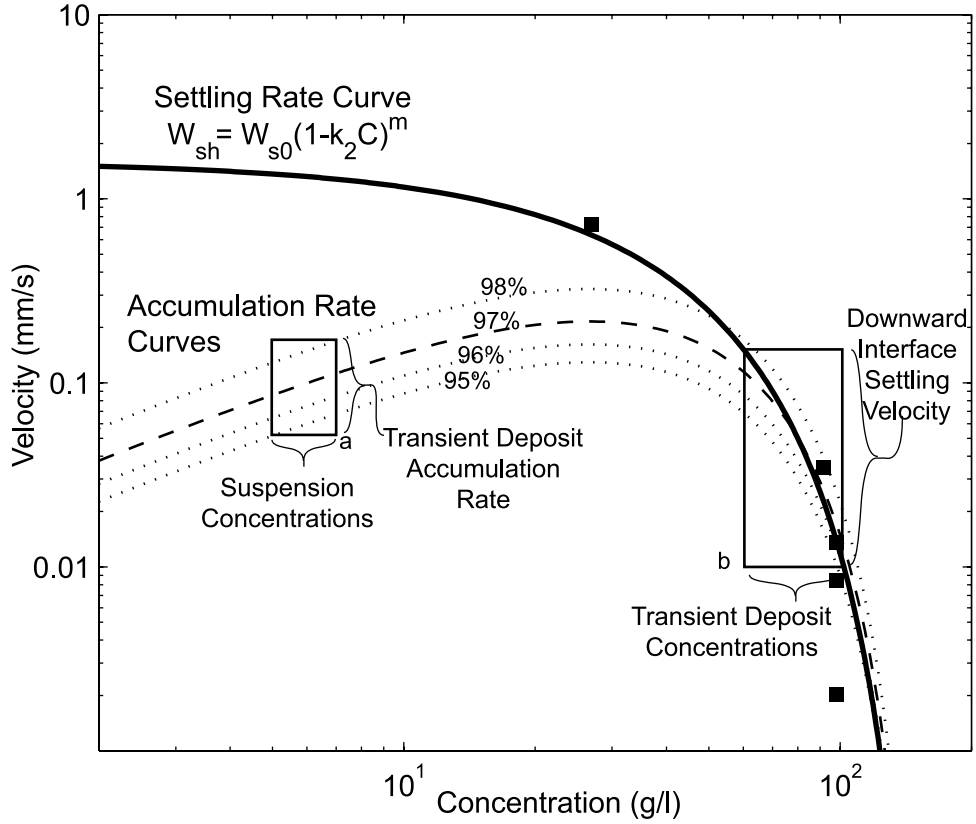

Figure 15. Settling rate of particles and of the mud-water interface from equation (1) (thick black line) fit to laboratory experimental data (squares). Also shown is the accumulation rate (upward velocity of the mud-water interface) based on several porosities (dashed lines). The settling rate times the concentration on the *x* axis, with various assumed porosities, is used to calculate the accumulation rate. Box a encloses the field-observed transient deposit accumulation rates of 0.05–0.2 mm s^{-1} based on the assumed porosities between 95 and 98% (vertical axis) for the observed suspension concentrations (horizontal axis) between 4 and 6 g L^{-1}. Box b encloses the field observed consolidation (hindered settling, vertical axis) rate of ~0.2 mm s^{-1} for the assumed transient deposit concentrations (horizontal axis) of 50–130 g L^{-1} (98–95% porosity).

[48] On the basis of this settling formulation, with near-bed suspended sediment concentrations below 10 g L^{-1}, the downward settling velocity of the sediment (w_{sh}) is ~1.5 mm s^{-1} (Figure 15). This large settling velocity is due to flocculation, as seen in the LISST data (Figure 11), and is consistent with previous estimates of floc settling velocities in estuaries [*Fugate and Friedrichs*, 2002]. This settling velocity combined with ABS measured near-bed concentrations of 4–6 g L^{-1} results in an estimate of the downward flux of sediment. Using a one-dimensional balance between downward flux and accumulation rates (i.e., the accumulation is solely due to flux from above and not lateral advection), the downward flux predicts accumulation rates of between 0.05 and 0.2 mm s^{-1} based on the assumed porosities between 95 and 98% (box a in Figure 15). The ABS measured accumulation rate values of 0.006–0.17 mm s^{-1} (Figure 10) are consistent with the predictions.

[49] Settling velocities of order 1 mm s^{-1} are required to maintain the high downward flux sufficient to make the fluid mud layer accumulate at the observed rate. This settling velocity is consistent with the flocculation observed in the LISST data (Figure 11). At lower concentrations, on the order of several hundreds of milligrams per liter, other studies [e.g., *Schubel et al.*, 1978] have shown that variation in flocculation on the tidal timescale is not required to produce their observed downward flux rates. In this study, with higher concentrations of grams per liter, there is direct evidence from the LISST data for flocculation on the tidal timescale, and it is required to produce a flux rate consistent with the observations. Thus the combination of flocculation and convergence is required to form the observed deposits.

[50] An alternative hypothesis to the water column convergence is that a pool of fluid mud is created at a location other than our measurement site and then is laterally advected under the tripod as mobile fluid mud, forced by either gravity or friction from tidal currents in the water column. Bed slopes for gravitational forcing are relatively low, <0.001 in the along-channel direction and 0.005 in the across-channel direction. Unfortunately, we do not have velocity data in the fluid mud layer to unequivocally determine if the fluid mud is moving. Whether or not the fluid mud was advected to the tripod location, in either case a trapping mechanism is required for the formation of the fluid mud layer. Because of the coincidence of the frontal location with the observed growth of the fluid mud layer, and because our calculations show that there is a sufficient

downward flux of sediment to the fluid layer from the suspension above, it appears that the above explanation of local trapping is most consistent with the observations. The burst-sampled acoustic backscatter data also indicate that the fluid mud is stationary. In other environments, where moving fluid mud was observed by an ABS, small-scale waves on the mud-water interface were observed [*Traykovski et al.*, 2000]. In the Hudson ABS data the interface does not show any small-scale waves.

5.1.3. Accumulation of Consolidated Sediment

[51] The ABS observations (Figure 10) indicate a gradual reduction in the thickness of the transient deposit, starting close to slack water and continuing to the time of maximum flood. The overlying water has no suspended sediment during the beginning of this period, indicating that the initial decrease in layer elevation is due to dewatering and consolidation. The rate of consolidation, $\sim$0.02 mm s^{-1}, is consistent with laboratory observations (Figure 3) for concentrations on the order of 100 g L^{-1} (box b in Figure 15). As flood tidal velocities increase, some sediment is eroded away by local resuspension. If this local resuspension is insufficient to remove all the sediment that was deposited during the previous ebb, a net deposit of several centimeters can form. As discussed in section 5.1.2, estimates of porosity relative to estimates of flux convergence suggest that erosion removes a relatively small percentage of the deposit on cycles that accumulate sediment.

[52] The tidal cycles that leave behind deposits $\geq$1 cm appear to have slightly lower flood velocities on average, thus reducing the tendency for erosion of the recently deposited layer (Figure 16). These tidal cycles also show the highest suspended concentration during ebb and the lowest concentration during flood, which also increases the potential for preservation of the transient deposits. However, the variations in deposition are relatively large ($\sim$10 cm in a phase average of events that deposit >1 cm of sediment) in spite of only small differences in velocity. One possibility is that the exact location of the deposition is very sensitive to the interactions between tidal asymmetry and the location of the salinity front.

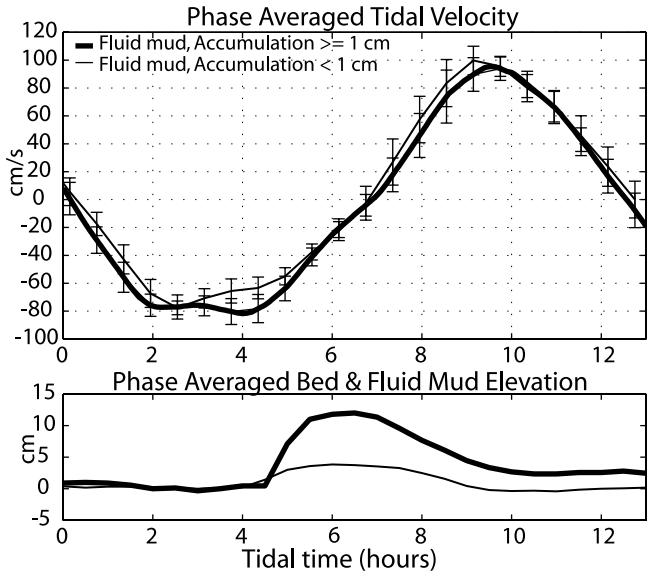

Figure 16. (top) Tidal phase coherent averages of ADCP velocity measured 2.5 mab. (bottom) Bed elevation estimates from the ABS. Averages over events with fluid mud and net accumulation over 1 cm (thick lines) and averages over events with fluid mud and net accumulation less than 1 cm (thin lines) are shown. The averaging was performed over the depositional period from 26 May to 5 June. The solid lines include the averages of nine ebb events with fluid mud and net accumulation over 1 cm during this period, while the dashed lines include 18 ebb cycles with fluid mud and net accumulation <1 cm.

5.2. Relation of Fine-Scale Stratigraphy to Deposition and Erosion Processes

[53] The comparison of optical and acoustic measurements of suspended sediment provides an indication of the grain size variations, which helps explain how the tidal variations in deposition and erosion lead to the observed fine-scale stratigraphy. Acoustic backscatter is most sensitive to coarser particles, and the optical sensor is most sensitive to the finest particles; thus the relative magnitudes of OBS- and ABS-derived suspended sediment concentration data can be used as a proxy for particle size [*Lynch et al.*, 1994]. The LISST instrument also provides an estimate of particle size and measures the aggregated particle size for flocs, unlike the ratio of ABS/OBS data, which is thought to more closely follow the primary particle size. Figure 17 includes phase averages of optical and acoustic data over nine tidal cycles that accumulated >1 cm of sediment during the period of high deposition. These data were used to determine the tidal variation of grain size and how it relates to the stratigraphy. Averages were performed in a bed- referenced coordinate system because the bed changes elevation from one tidal cycle to the next. The transient fluid mud deposits were considered to be part of the bed for the purposes of averaging suspended sediment concentrations, and the concentrations were estimated using ABS and OBS data at 10 cm above the sediment-water interface.

[54] During the early ebb, when the conditions are slightly erosional, finer particles dominate. On the basis of the LISST data taken during neap tides under nontrapping conditions, these particles are probably small aggregates (25–80 μm). From maximum ebb to late ebb, when sediment trapping occurs and there is rapid accumulation of fluid mud, the suspension contains more coarse particles based on the ratio of the ABS/OBS data and on large aggregates (125–500 μm) observed in the LISST data. During the entire flood, when significant erosion occurs, finer particles are observed. Thus the suspended sediment was found to be finer during erosional periods, and it only appears coarser during the period of sediment trapping and rapid deposition. The vertical gradients in sediment concentration shown in the lower panels of Figures 17c and 17d also suggest coarser particles during ebb. During ebb, there is a vertical gradient in both the ABS- and OBS-derived suspended sediment concentration data, with the ABS data showing a stronger gradient as it is sensitive to the large particles. The larger particles are expected to have stronger gradients due to their higher settling velocity relative to upward diffusive mixing. During flood, both sensors show weak gradients, indicating finer particles, and the magnitude

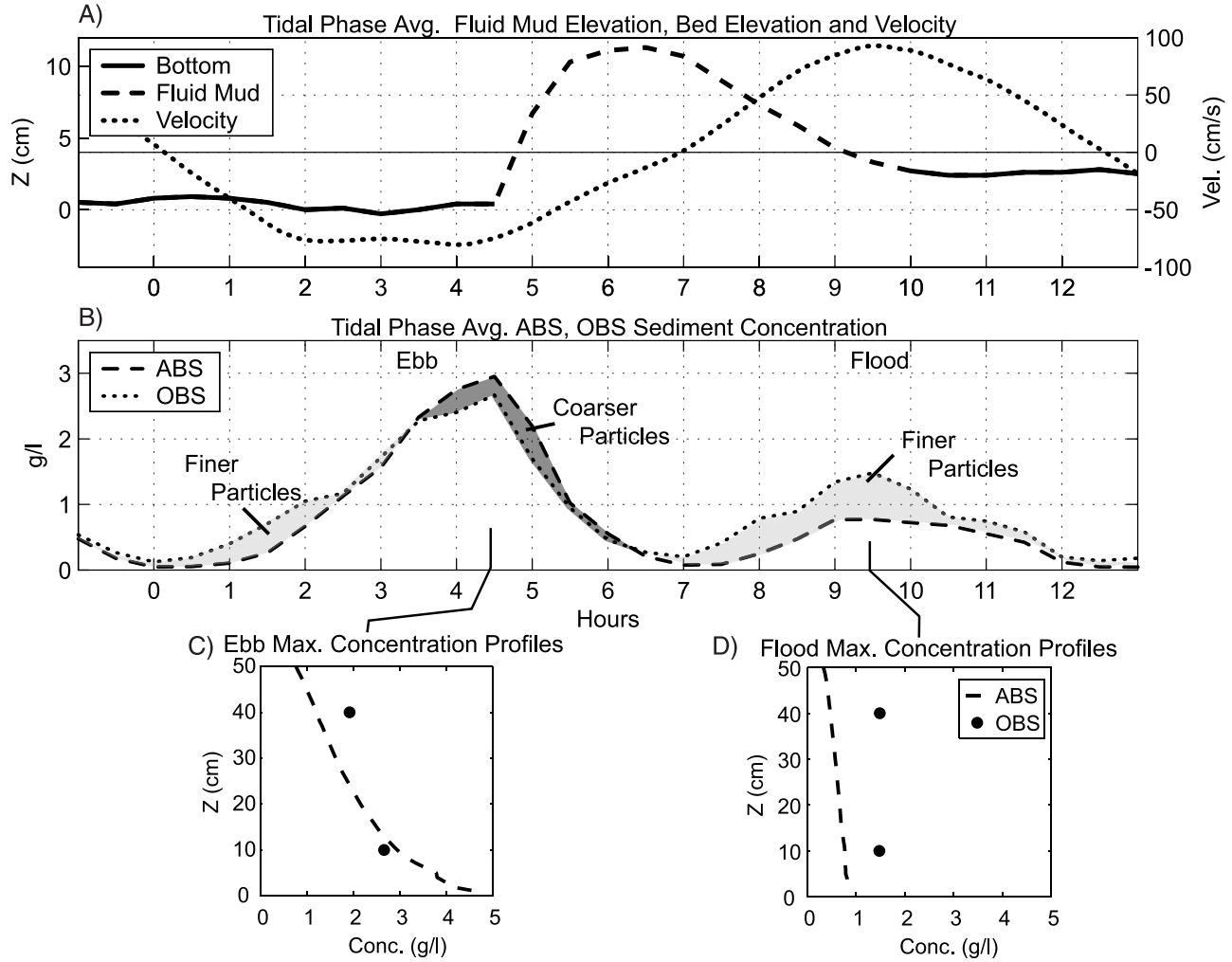

Figure 17. (a) Phase-averaged bed elevation, fluid mud, and velocity for tidal cycles with >1 cm of mud accumulation during the period of high deposition from 26 May to 5 June. (b) Phase-averaged ABS and OBS suspended sediment concentration estimates from 20 cmab for the same tidal cycles as in Figure 17a. (c, d) Vertical profiles of suspended sediment concentration estimates from the ABS (dashed line) and OBS (dots) at maximum concentration during ebb and flood.

of the ABS data are lower than that of the OBS data, also indicating finer particles.

[55] On the basis of these data, we suggest that both fine and coarse sediment, perhaps flocculated together into single particles, are delivered to the fluid mud deposits during the ebb depositional phase, whereas fines are preferentially eroded during flood and the beginning of the subsequent ebb. Thus the homogenous clayey silt beds are a product of ebb deposition that has not been sorted by subsequent erosion during flood. The subsequent erosion during the flood and early ebb preferentially erodes the fines, producing fine sand and silt laminae at the tops of the surviving layers of ebb deposition. The acoustic penetration into the fluid mud (Figure 10e) shows a layer of higher scattering 10 cm below the water fluid mud interface that could also be due to grain size sorting introduced during deposition or the first stages of settling of the fluid mud layer.

[56] Cores taken in the southern depositional area show beds of homogenous clayey silt with a thickness of 1–2 cm interspersed with thin (3–6 mm) laminae of fine sand to coarse silt. The laminae appear as lighter shades of gray (Figure 6, Figure 12, and Figure 18). The clayey silt beds are shown as darker shades of gray to black. The size dependence of the depositional processes versus the erosional process should leave layering that is consistent with the elevation changes observed by the acoustic sensor.

[57] The acoustic elevation changes are shown in Figure 18 along with a diver push core that was taken as close as possible to directly under the ABS. The tilted orientation of the layering is due to the coring device being inserted at an angle as there was barely enough room for a diver under the instrument frame. Erosional surfaces are identified in the ABS bed elevation time series by scanning backward in time and picking out progressive minima of the bed elevation. These surfaces are expected to be the very fine sand to coarse silt laminae that are the result of erosion. In between these laminae are the products of the depositional events seen as homogenous clayey silt beds. Since the period after 8 June was erosional

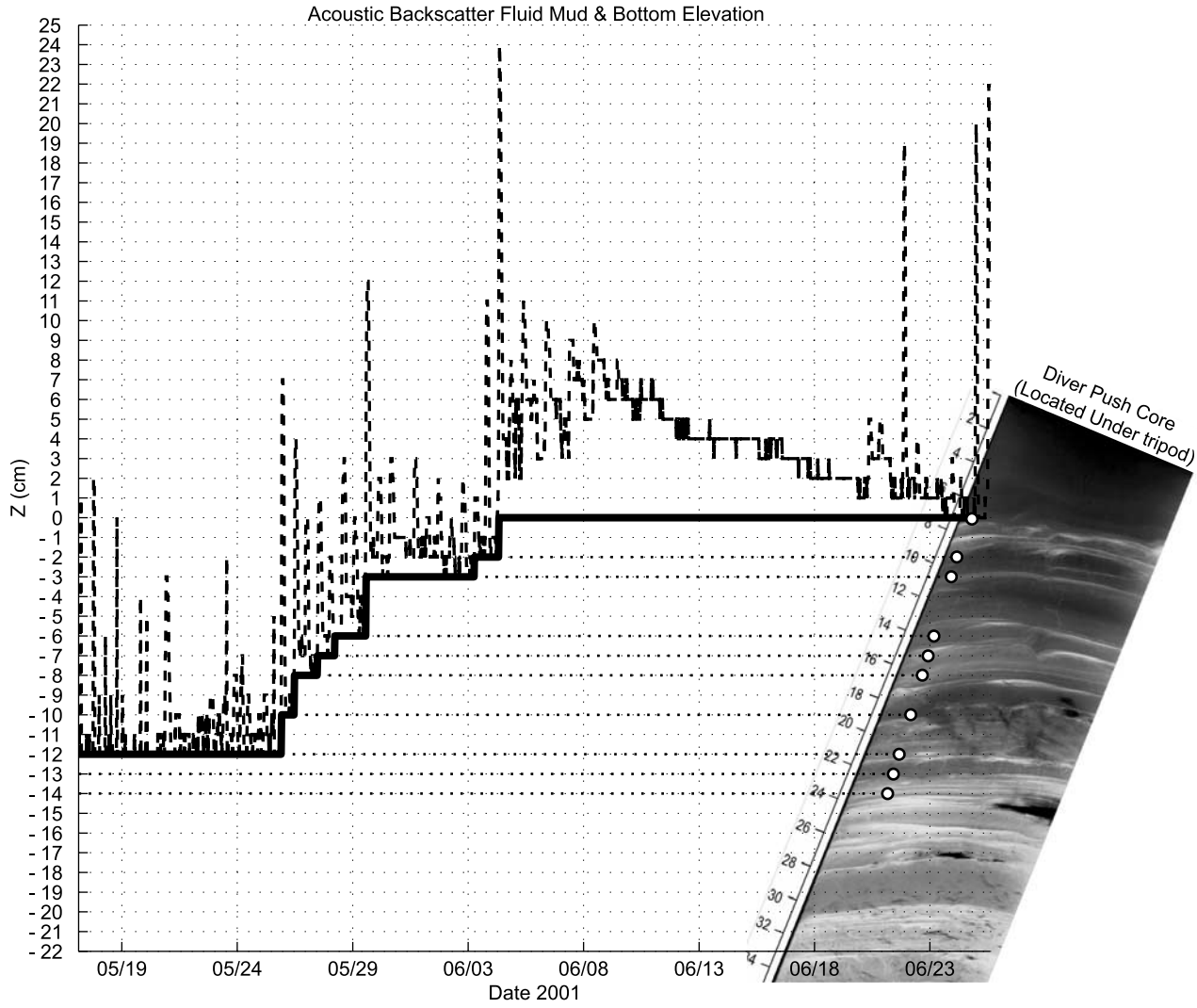

Figure 18. (left) Elevation of the bed (thin solid line) and the fluid mud transient deposit (dashed line) from ABS data. The thick black line (with dotted lines to align surfaces to the core) represents consecutive erosional surfaces that could potentially been seen in a core as fine sand to coarse silt laminae. (right) An X-radiograph negative from a core taken directly under the tripod during recovery aligned with the ABS elevation data.

(6 cm decrease between 8 and 25 June), the top of the uppermost interlaminated bed in the core, at 8 cm on the core depth scale, was aligned with the final erosional surface evident in the ABS data at 0 cm on the ABS depth scale. Above this surface, there was a several centimeter thick layer of fluid mud, which is also visible in the core taken adjacent to the tripod (Figure 12).

[58] Comparing the cores in Figure 12 (adjacent to the tripod) and Figure 18 (under the tripod), it would appear that the core taken adjacent to the tripod has slightly less erosion than the core taken under the tripod. The features from 7 to 14 cm in the core adjacent to the tripod are aligned with features from 8 to 14 cm (core depth scale) in the core under the tripod. However, there is an additional interlaminated bed in the core adjacent to the tripod between the fluid mud-sediment interface at 4 and 7 cm that is not present in the core under the tripod, perhaps due to enhanced erosion under the tripod.

[59] While the ABS bed elevation record is not able to match the exact layering present in the core, many of the elevation changes in the ABS record are reflected in the bedding. A similar overall structure is present in both records. The thicker homogenous clayey silt beds appear to have resulted from large deposition during ebb followed by floods with smaller erosion. One particular example of this is the homogenous bed between 11 and 14 cm (core depth scale) in the core under the tripod (Figure 18) that could be the result of a 3 cm net depositional event recorded by the ABS on 30 May. These thicker homogenous beds are interspersed with thinner beds consisting of laminae of clay and silt that appear to be the result of ebb tide deposition that is nearly matched by flood erosion. The exact mechanism for the sorting of coarse silt and very fine sand into thin lamina (Figure 12) is most likely some combination of sorting during deposition and during erosion. Most of the sorting probably occurs during erosion, as indicated by the prefer-

ential erosion of fine material, but there could potentially also be sorting during deposition as the coarser particles could be deposited earlier in the tidal cycle.

6. Conclusions

[60] This data set has produced a clear record of the transport processes leading to the observed fine-scale stratigraphy, often referred to as tidalites, in the ETM of the Hudson River estuary. The data show that the layering is produced entirely during spring tides, and the variation in thickness of individual beds (centimeters) and laminae (millimeters) reflects the amount of sediment that was deposited in the ebb portion of the tidal cycle relative to the amount of dewatering and erosion during flood. These results differ from those of previous studies, which explain the differences in bedding as being due to different amounts of deposition in spring versus neap tides or varying deposition under flood and ebb. Here larger-scale patterns (larger than several cm) can be attributed to differences between individual ebb tidal cycles during spring tides as some produce many thick layers and others do not.

[61] The data also reveal how tidal asymmetry plays an important role in determining the structure of the deposits. Combined optical and acoustic measurement of suspended sediment and bed elevation show that transient deposits of fluid mud are formed as both coarser and fine particles are deposited during decreasing ebb. Fine sediments are then preferentially resuspended during flood. The magnitude of the transient deposits (10–25 cm) is usually an order of magnitude greater than the net accumulation of 1–4 cm after deposition, settling, and erosion in a single ebb to flood tidal cycle. A succession of 7 to 10 of these depositional events occur during 1 to 2 spring tidal cycles to form a seasonal deposit of tens of centimeters, with internal bedding reflecting the formative processes. This view of the temporal dependence of the deposition process and the resulting fine-scale stratigraphy should provide a useful case study for tidal depositional environments where process observations are not available.

[62] Significant questions remain about the timing of the major depositional events and the trajectory of the incoming sediment. Although it is believed that most of the new sediment enters the estuary during the freshet, the deposition events occurred 1.5–2 months later. Also, it was not clear why the large depositional events occurred on one particular tidal cycle with little deposition occurring on adjacent tidal cycles with nearly the same flow conditions. These observations indicate a spatially and temporally complex interaction between the flow and the sediment deposition processes.

[63] **Acknowledgments.** The authors would like to acknowledge the Hudson River Foundation, who provided funding for this work under grant 009/00A. We also thank Gail Kineke, who reviewed a draft of this paper. Jay Sisson, Craig Marquette, and Glenn McDonald helped with the instrumentation, tripods, and moorings used to take the measurements. This is Woods Hole Oceanographic Institution contribution 11016.

References

Feng, H., J. K. Cochran, and D. J. Hirschberg (1999), ^{234}Th and ^{7}Be as tracers for the sources of particles to the turbidity maximum of the Hudson River estuary, *Estuarine Coastal Shelf Sci.*, *49*(5), 629–645.

Fugate, D. C., and C. T. Friedrichs (2002), Determining concentration and fall velocity of estuarine particle populations using ADV, OBS and LISST, *Cont. Shelf Res.*, *22*, 1867–1886.

Geyer, W. R. (1993), The importance of suppression of turbulence by stratification on the estuarine turbidity maximum, *Estuaries*, *16*(1), 113–125.

Geyer, W. R., R. P. Signell, and G. C. Kineke (1998), Lateral trapping of sediment in a partially mixed estuary, in *Physics of Estuaries and Coastal Seas*, edited by J. Dronkers and M. B. A. M. Scheffers, pp. 115–124, A. A. Balkema, Brookfield, Vt.

Geyer, W. R., P. Hill, T. Milligan, and P. Traykovski (2000), The structure of the Eel River plume during floods, *Cont. Shelf Res.*, *20*, 2067–2093.

Geyer, W. R., J. D. Woodruff, and P. Traykovski (2001), Sediment transport and trapping in the Hudson River estuary, *Estuaries*, *24*(5), 670–679.

Gibbs, R. J., D. M. Tshudy, L. Konwar, and J. M. Martin (1989), Coagulation and transport of sediment in the Gironde estuary, *Sedimentology*, *36*, 987–999.

Gibbs, R. J., P. K. Jha, and G. J. Chakrapani (1994), Sediment particle size in the Hudson River estuary, *Sedimentology*, *41*, 1063–1068.

Glangeaud, L. (1938), Transport et sedimentation dans l'estuarie de la Gironde (caracteres petrographiques des formations fluviatiles, suamtres, littorals et neritiques), *Bull. Geol. Soc. Fr.*, *8*, 599–630.

Hori, K., Y. Saito, Q. Zhao, X. Cheng, P. Wang, Y. Sato, and C. Li (2001), Sedimentary facies of the tide dominated paleo-Changjiang (Yangtze) estuary during the last transgression, *Mar. Geol.*, *177*, 331–351.

Jaeger, J. M., and C. A. Nittrouer (1995), Tidal controls on the formation of fine-scale sedimentary strata near the Amazon River mouth, *Mar. Geol.*, *125*, 259–281.

Lick, W., and H. Huang (1993), Flocculation and the physical properties of flocs, in *Nearshore and Estuarine Cohesive Sediment Transport*, *Coastal Estuarine Stud.*, vol. 42, edited by A. J. Mehta, pp. 21–39, AGU, Washington, D. C.

Lynch, J. F., J. D. Irish, C. R. Sherwood, and Y. C. Agrawal (1994), Determining suspended particle size information from acoustical and optical backscatter measurements, *Cont. Shelf Res.*, *14*, 1139–1164.

Meade, R. H. (1969), Landward transport of bottom sediments in estuaries of the Atlantic Coastal Plain, *J. Sediment. Petrol.*, *39*, 222–234.

Nittrouer, C. A. (1999), STRATAFORM: Overview of its design and synthesis of its results, *Mar. Geol.*, *154*, 3–12.

Partheniades, E. (1965), Erosion and deposition of cohesive soils, *J. Hydrol. Div. Am. Soc. Civ. Eng.*, *91*(HY1), 105–139.

Postma, H. (1967), Sediment transport and sedimentation in the estuarine environment, in *Estuaries*, edited by G. H. Lauff, pp. 158–179, Am. Assoc. Adv. Sci., Washington, D. C.

Richardson, J. F., and W. N. Zaki (1954), The sedimentation of a suspension of uniform spheres under conditions of viscous flow, *Chem. Eng. Sci.*, *3*, 65–72.

Ross, M. R., and A. J. Mehta (1989), On the mechanics of lutoclines and fluid mud, *J. Coastal Res.*, *5*, 51–61.

Sommerfield, C. K. (2003), Mechanisms of sediment deposition, erosion, and long-term accumulation in the Hudson estuary, final report, 42 pp., Hudson River Found., New York.

Thorne, P. D., P. J. Hardcastle, and R. L. Soulsby (1993), Analysis of acoustic measurements of suspended sediments, *J. Geophys. Res.*, *98*, 899–910.

Traykovski, P., W. R. Geyer, J. D. Irish, and J. F. Lynch (2000), The role of wave-induced density-driven fluid mud flows for cross-shelf transport on the Eel River continental shelf, *Cont. Shelf Res.*, *20*, 2113–2140.

Wellershaus, S. (1981), Turbidity maximum and mud shoaling in the Weser estuary, *Arch. Hydrobiol.*, *92*, 161–198.

Wheatcroft, R. A., and J. C. Borgeld (2000), Oceanic flood deposits on the northern California shelf: Large-scale distribution and small-scale physical properties, *Cont. Shelf Res.*, *20*, 2163–2190.

Winterwerp, J. C. (2002), On the flocculation and settling velocity of estuarine mud, *Cont. Shelf Res.*, *22*, 1339–1360.

Woodruff, J. D., W. R. Geyer, C. K. Sommerfield, and N. W. Driscoll (2001), Seasonal variation of sediment deposition in the Hudson River estuary, *Mar. Geol.*, *179*, 105–119.

R. Geyer and P. Traykovski, Applied Ocean Physics and Engineering Department, MS #11, Woods Hole Oceanographic Institution, Woods Hole, MA 02543, USA. (rgeyer@whoi.edu; ptraykovksi@whoi.edu)

C. Sommerfield, College of Marine Studies, University of Delaware, 700 Pilottown Road, Lewes, DE 19958-1298, USA. (cs@udel.edu)